

**DEVELOPMENT OF NOVEL ALLOYS FOR USE AS HYDROGEN
PURIFICATION MEMBRANES**

by

CHARALAMPOS ANASTASIADIS

A thesis submitted to the University of Birmingham for the degree of

MASTER OF RESEARCH

Hydrogen Materials Group

School of Metallurgy and Materials

University of Birmingham

December 2010

UNIVERSITY OF
BIRMINGHAM

University of Birmingham Research Archive

e-theses repository

This unpublished thesis/dissertation is copyright of the author and/or third parties. The intellectual property rights of the author or third parties in respect of this work are as defined by The Copyright Designs and Patents Act 1988 or as modified by any successor legislation.

Any use made of information contained in this thesis/dissertation must be in accordance with that legislation and must be properly acknowledged. Further distribution or reproduction in any format is prohibited without the permission of the copyright holder.

Abstract

During the production of hydrogen a number of other elements are also produced, removing these elements is crucial for the production of pure hydrogen.

Due to their potentially infinite hydrogen selectivity, dense-metal membranes are a very promising method for separating hydrogen; currently the metallic membranes commonly used are based on Pd-Ag alloys.

Although palladium possesses a very active surface for hydrogen absorption and desorption, other metals such as the transition metals (e.g vanadium (V), tantalum (Ta) and niobium (Nb)) exhibit greater hydrogen permeability. In addition, these metals are much less costly than palladium, therefore offering considerable improvements in performance at lower cost. However, both vanadium and niobium form stable surface oxides and do not possess the catalytic abilities of palladium [1, 2], adversely affecting the observed permeability. Coating a thin film of palladium on each side of the potential membranes such as vanadium or niobium could potentially solve this surface problem, making the fabrication of cheaper and more effective membranes feasible [1, 3].

Besides being used as the core material for membrane vanadium can also be considered as a candidate for use as an interdiffusion barrier in palladium supported membranes. Substrates such as porous stainless steel can be used to fabricate membranes with minimum palladium thicknesses. However, at high temperatures these types of membranes experience Pd / Fe interdiffusion into the substrate thus changing the initial properties of the membrane. Due to the higher melting point of vanadium, when compared to palladium and its good hydrogen permeability, vanadium can be considered a very good candidate for blocking this effect.

Acknowledgements

I would like to express my gratitude to all the people that their help from the most trivial to the most consequential lead to the completion of this work.

To my supervisor Dr David Book for all its help in all the aspect of my postgraduate program, to Professor Rex Harris and Dr John Speight whose experience and knowledge was always available to me. Also a special thanks to Sean Fletcher whose help and guidance was crucial to overcome the difficulties I came across.

I would also like to mention all the friendly people I met in lab 11 Dr Alan Walton, Dr Vicky Mann, Dr Alex Bevan, Dr Ruixia Liu, Dan, Rob, Steve, Yinghe, David, Miha, Sal, Danny and Daniel.

Finally few words for my family, their love and encouragement throughout the year was always present and strong, without their support I could have never materialized my intention for this program and for that I am grateful.

Contents

| | |
|--|-----------|
| 1 Introduction | 1 |
| 1.1 An overview..... | 1 |
| 1.2 Drive towards a hydrogen economy | 3 |
| 1.3 Hydrogen production..... | 5 |
| 1.3.1 Water..... | 5 |
| 1.3.1.1 Water electrolysis..... | 5 |
| 1.3.1.2 Thermochemical splitting of water..... | 8 |
| 1.3.1.3 Photoelectrolysis..... | 9 |
| 1.3.2 Hydrocarbons..... | 10 |
| 1.3.2.1 Reformation of natural gas..... | 10 |
| 1.3.2.2 Gasification of coal..... | 11 |
| 1.3.2.3 Biomass..... | 12 |
| 1.4 Fuel cells..... | 14 |
| 1.5 Need for hydrogen purification..... | 16 |
| 2 Literature Review | 18 |

| | |
|--|-----------|
| 2.1Hydrogen Separation..... | 18 |
| 2.1.1Pressure swing adsorption..... | 18 |
| 2.1.2Cryogenic distillation..... | 20 |
| 2.2Hydrogen separation membranes..... | 20 |
| 2.2.1Porous membranes..... | 21 |
| 2.2.2Dense membranes..... | 22 |
| 2.3Solution diffusion mechanism..... | 23 |
| 2.4Palladium based membranes..... | 28 |
| 2.5Novel materials for the fabrication of dense metallic membranes | 31 |
| 2.5.1Niobium hydrogen and Vanadium hydrogen systems..... | 34 |
| 2.6Literature Review summary..... | 35 |
| 2.7Project aims..... | 36 |
| 3Experimental Approach | 37 |
| 3.1Preparation of Pd Coated V and Nb Foils..... | 37 |
| 3.2Preperation of stainless steel (SS) discs..... | 38 |
| 3.3Coating Process..... | 38 |
| 3.4Confocal laser microscope..... | 41 |
| 3.5Scanning Electron Microscopy(SEM)..... | 43 |
| 3.6 Material characterization..... | 43 |

| | |
|--|-----------|
| 3.7Hydrogen permeability apparatus..... | 45 |
| 4Results and Discussion | 49 |
| 4.1Pd-V-Pd..... | 49 |
| 4.1.1Material characterization..... | 49 |
| 4.1.2Hydrogen Permeability measurements..... | 54 |
| 4.2PD-Nb-Pd..... | 65 |
| 4.3Permeability comparison between Pd, PdAg, and Pd-V-Pd membranes..... | 68 |
| 4.4Stability measurement..... | 69 |
| 4.5SS couples (SS-Pd and SS-V-Pd)..... | 70 |
| 4.6SEM investigation..... | 72 |
| 4.7General discussion..... | 75 |
| 5Conclusions and further work | 76 |
| 5.1Conclusions..... | 76 |
| 5.2Future work..... | 77 |
| Bibliography | 78 |

Chapter 1

Introduction

1.1 An overview

For more than a century fossil fuels have been the major energy source, today issues such as the depletion of reserves and greenhouse gas emissions (CO_2 , CH_4 , N_2O , SF_6), associated with the use of fossil fuels have made clear that the transition to a new energy system is essential.

During the last two centuries CO_2 quantities in the atmosphere have increased dramatically resulting the climate changes earth has face over the last century. If CO_2 emissions continue to rise at the current rate, the effects for our planet could be catastrophic. Also the predictions for the hydrocarbon energy system are not optimistic, fuel reserves have already reach their peak and the predictions are that oil, coal and natural gas which are the main energy sources used today have a expected lifetime of 50 100 and 150 years respectively{USA department of energy predictions). These predictions are assuming that no new reserves are found and that the consumption rate is going to remain stable, however, the prediction for world energy consumption rate is not bright as the prognosis is that by 2050 consumption is going to be almost double[4, 5].

Today people around the world consume about 13 TW of energy, mainly produced from fossil fuels. In order to satisfy this huge and growing need for energy but also keep atmospheric CO₂ concentration stable in the years to come, 10 TW of carbon neutral/free energy must be produced by mid-century, while a decrease of CO₂ at 350 ppm would require the production of over 30 TW of carbon free energy[6].

One of the most promising solutions to replace hydrocarbons and produce carbon/free energy is hydrogen. In the future it is likely that hydrogen will play a major role as an energy carrier and will eventually replace the current hydrocarbon-based energy economy. In pure form, the energy content of hydrogen can be released either through a hydrogen internal combustion engine or through a hydrogen fuel cell system. Between these two solutions, combining hydrogen with fuel cells is the most clean and efficient way to exploit it. Inside a hydrogen fuel cell the energy content of hydrogen is released in the form of electricity as the result of hydrogen reacting with oxygen and that without the production of any harmful emission as the only byproduct is water.

However, in Nature, molecular hydrogen is only found in trace amounts; as it exists in the form of more complex compounds such as hydrocarbons or water. Thus before hydrogen can be used as an energy carrier it must be first liberated.

Along with the extraction of hydrogen, a number of other substances are also released creating a gas mix that can't be used in the high purity-demanding applications that hydrogen is currently used for. Also hydrogen fuel cell requires hydrogen feed of extra high purity in order to avoid contamination that can lead to pure performance.

Currently most hydrogen produced comes through large petrochemical and chemical factories as a byproduct while its purification is mainly done through pressure swing absorption (PSA) [7]. The primary consumer for hydrogen doesn't come from the energy

sector; the majority of hydrogen is used in refineries for applications such as hydro-desulphurization of fuels and hydro-cracking. A large amount is also used in the production of a variety of products e.g. semiconductors, steel alloys, methanol, vitamins and textiles. Lastly hydrogen is also used for the recycling of rare earth magnets[5, 8].

The high constant need of energy, moderate purity of hydrogen produced as well as the limitation of use only in large scale operations make PSA unattractive as the primary hydrogen purification method of a hydrogen energy system.

Metallic membranes can work with very good efficiencies, have low demands in energy, are reasonably easy to make while they can work at both large and small scale. The material most often used for hydrogen purification membranes is Pd-Ag alloys but issues like the cost of the commodity have brought up the need for new materials that can replace palladium alloys and if that is possible to improve the qualities of hydrogen purification.

Two materials that can replace palladium are vanadium (V) and niobium (Nb), as they have much higher hydrogen permeabilities values in comparison to palladium [1-3]. These two materials were tested and are going to be discussed as replacement for Pd in this thesis.

1.2 Drive towards a Hydrogen Economy

Recent research has revealed that the concentration of CO₂ in the atmosphere today is similar to that of 15 to 20 million years ago. At that time in earth's history the atmosphere was very warm while the sea level was one meter higher than it is today[9]. This research, only one of many every year published, makes it very clear that the relationship between

earth climate and CO₂ as well as what the future of the Earth will be if we continue releasing CO₂ gas at the rate we do now.

Since the world realized the importance of the problem, a debate has started about the best way to resolve it. One of the outcomes of this debate has resulted in the creation of a framework by UNITED NATIONS known as the Kyoto protocol. Countries from all over the world that have signed the protocol were automatically obliged to follow a number of rules that will result in the gradual decrease in greenhouse gas emission [10]. The introduction of renewable and clean energy sources is one of the Kyoto protocol's main policies; and one of the most promising and long term solutions for the reduction of greenhouse gases is the use of hydrogen as an energy carrier.

In order for hydrogen to be established as one of the main energy provider for our needs, a number of different scientist are collaborating in order to address issues related to hydrogen production, storage, supply and utilisation. This system that has hydrogen in its centre is called a hydrogen economy.

Currently the hydrogen economy is mostly linked with hydrocarbons either as a by-product during the production of fossil fuels or as a necessary ingredient for the production of petrochemical products. These limitations to large scale applications that are not hydrogen energy related are due to the currently prohibitively high cost of a hydrogen energy system for commercial use.

The most common concept of how a hydrogen economy will look in the future is that of hydrogen acting as a supplementary energy carrier along with renewable energy sources such as wind or solar helping to minimise the intermittency problems associated with these energy sources.

The cost of hydrogen production and of fuel cells, are the two major obstacles that drive the research on reaching cost targets in order for the establishment of a hydrogen energy system to be possible. Decreasing hydrogen production and fuel cells costs by four and ten times respectively are the current targets [5].

1.3 Hydrogen production

The main sources for the production of hydrogen are water and hydrocarbons. Hydrocarbons most common used today as raw materials for hydrogen production are natural gas, oil, coal and biomass.

1.3.1 Water

1.3.1.1 Water electrolysis

When electric current passes through water, hydrogen can be released in a process called water electrolysis. During this process, water is decomposed into its basic elements oxygen and hydrogen.

Two electrodes are placed in the water in order for the current to pass through it, and initiate the reactions necessary for the decomposition of water. The main electrolysis used are alkaline, proton exchange membrane (PEM) and solid oxide electrolysis cells (SOEC), the

two electrodes are called cathode (negative charged) and anode (positive charged) and are made from different materials for each electrolyzer.

Alkaline-based electrolysis consists of a micro-porous separator and an alkaline solution of KOH or NaOH about 30wt%. The material used for the two electrodes are nickel with a catalytic layer such as platinum for the cathode, while anode consists from either nickel or copper with a metal oxide coating like manganese , tungsten or ruthenium[11].

Alkaline electrolysis begins with the introduction of water in the cathode. There water is decomposed into H₂ and OH. Then OH travels through the alkaline solution to the anode where oxygen is created.

The reactions that take place in the two electrodes are:



A PEM electrolyzer consists of a membrane made of Nafion that separates the two electrodes. It only allows protons to come through it and also separates the two gases. Both electrodes are usually made of Pt black, iridium, ruthenium and rhodium[11].

Here water is introduced at the anode. There water splits into protons and oxygen; protons use the Nafion membrane to travel to the cathode where they are recombined into hydrogen.

The reactions taking place are:



Lastly, SOEC requires thermal energy along with electricity, and they can operate at high temperatures. These all use a solid oxide electrolyte made of yttria stabilized zirconia, while anode and cathode are made of nickel containing yttria stabilized zirconia and metal-doped lanthanum metal oxides respectively[11]. The need for high temperatures can be solved if SOEC is combined with advanced high temperature nuclear reactors. Similar to the two previous types of electrolysis the reactions at anode and cathode are:



Electrolysis must be utilized along with sustainable energy sources if it is to produce zero CO₂ emissions hydrogen. When used with current fossil fuel based technologies, it will not

only produce CO₂ emissions but the cost will also be high. Efficiencies for the three types of electrolysis mentioned above are 50%-60% , 55%-70% , and 60% respectively[11].

Thus water electrolysis can produce hydrogen with zero carbon dioxide and for that is proposed as the future main method of hydrogen production. Currently the high cost as well as the not so good efficiency of the process limit the use of electrolysis to just 3,9% of the total world hydrogen production.

1.3.1.2 Thermo chemical splitting of water

When water is heated at a temperature over 2000 °C splits into hydrogen and oxygen. This process is called thermo-chemical water splitting or thermolysis. The high temperature needed for the rapid recombination of hydrogen with oxygen as well as the lack in abundance in materials that are stable at that high temperature lead to a number of thermal chemical cycles that have been identified in order to break water in separate steps and at lower temperatures. One of the most prominent thermo chemical cycles proposed is that of sulphuric acid and hydrogen iodine.

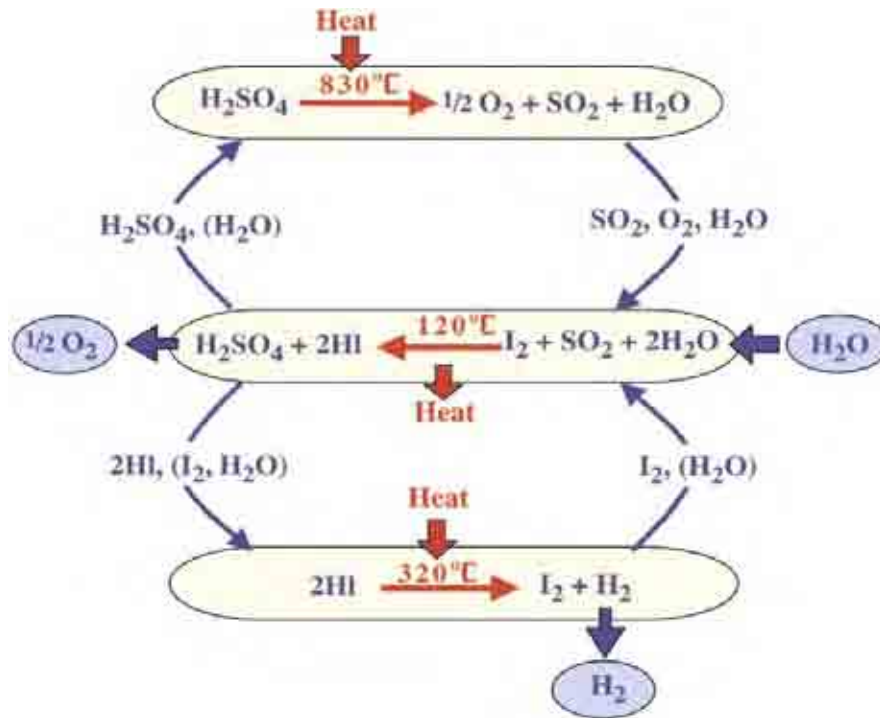


Figure 1 : Sulphur-Iodine cycle[12]

Low efficiency, high cost, corrosion of materials at high temperatures and lack of large scale production compared to other hydrogen production methods limit its current use to research level.

1.3.1.3 Photoelectrolysis

The combination of specific doped semiconductors along with sunlight and an aqueous electrolyte can generate hydrogen in a similar way that electrolysis does with a direct use of

sunlight. Extrinsic semiconductor materials of either n or p type can be used similar to photovoltaic. For example when sunlight (photons) hits an n-type based photoelectric cell inserted in an aqueous electrolyte it will create an electron-hole pair, holes will decompose water into hydrogen ions and oxygen gas at the anode side of the cell, electrons and hydrogen will travel to cathode the first via an electrical connection while ions will travel through the electrolyte, ions and electrons at anode will react and form hydrogen gas.

Photoelectrolysis is a very promising method for hydrogen generation but currently the efficiencies observed utilizing this method are very low. Some semiconductor materials being investigated for photoelectrolysis are WO_3 , Fe_2O_3 , n-GaAs, n-GaN, CdS, CIGS/Pt, p-InP/Pt[11].

1.3.2 Hydrocarbons

1.3.2.1 Reformation of natural gas

Until CO_2 emission-free methods of producing hydrogen such as water electrolysis becomes cheaper, the most widespread way to produce hydrogen today is through steam reformation of natural gas, and according to USA Department of Energy, 48% of world production of hydrogen derives from this method.

Steam reformation is divided in two stages; in the first stage natural gas (methane) reacts with water steam at temperatures between 800 and 1100 °C, producing carbon monoxide and hydrogen as described in equation 1.10 [13].

1.10 Reformation of natural gas $\text{CH}_4 + \text{H}_2\text{O} \rightarrow \text{CO} + 3\text{H}_2$

The second stage is called water-gas shift reaction and in order for the efficiency of the process to be increased it usually takes place twice, once at a high temperature (high temperature shift reaction $\sim 350^\circ\text{C}$) and then at a lower temperature (lower temperature shift reaction $\sim 190\text{-}210^\circ\text{C}$). During the reaction, carbon monoxide reacts with water producing more hydrogen and carbon dioxide.

1.11 Water-gas shift reaction $\text{CO} + \text{H}_2\text{O} \rightarrow \text{CO}_2 + \text{H}_2$

The whole process can be summarized by:

1.12 Steam methane reformation reaction $\text{CH}_4 + \text{H}_2\text{O} \rightarrow \text{CO}_2 + 4\text{H}_2$

A typical composition of the gas coming from a SMR reaction like the one mention above is:

1.13 74.1% H_2 , 18.5% CO_2 , 6.9% CH_4 and 0.1% CO [5]

1.3.2.2 Gasification of coal

As mentioned previously, coal is the most abundant fossil fuel source in earth. Currently it is used mainly in intergraded gasification combined cycle power generation systems (IGCC) to produce syngas which through a gas turbine generates electricity; this method of producing electricity through coal has been proved to be more efficient and less polluting comparing to standard coal combusting systems. IGCC can be integrated with water gas

shift reactors and gas separators in order to produce hydrogen along with electricity; such a system has shown even higher energy efficiency and lower CO₂ emissions, while sequestration of CO₂ would be much cheaper in comparison to a system that only produce electricity [11, 14-16].

During coal gasification, coal is inserted in a pressurized reactor in the presence of steam and heat, causing coal to oxidize and produce syngas, a mixture of carbon monoxide, hydrogen, nitrogen and small amounts of other substances. In an IGCC to hydrogen system a part of syngas is not used to produce electricity. Instead it reacts with water in a water gas shift reaction for the production of hydrogen [11, 14-16] .

1.3.2.3 Biomass

Biomass can be considered to be a variety of resources like agricultural crops, industrial, agricultural and forestry wastes and residues. All of these can be used as a feed for hydrogen generation through thermochemical (gasification, pyrolysis) and biological (fermentation, photosynthesis) processes. During pyrolysis biomass is transformed into liquid, solid and gas by heating at high temperatures (around 500C°) in the absence of oxygen. Hydrogen rich products of pyrolysis are then steam reformed to generate hydrogen[11, 17]. Fermentation uses bacteria and small organism enzymes that break down biomass and ultimately generate hydrogen and CO₂. Some bacteria and algae can also be used to produce hydrogen with the aid of solar energy in the photosynthesis process [11, 17].

Because biomass can be cultivated, it can be considered as a renewable source, while the net emission of CO₂ is near zero as CO₂ released in the atmosphere during the procedure of hydrogen production was previously consumed from biomass during cultivation. Current issues for the use of biomass include the production of tar as byproduct, the relatively small efficiency as hydrogen content in biomass is only 6% meaning that huge areas must be converted from food production to energy production leading to humanitarian issues[17].

1.4 Fuel cells

Fuel cells are electrochemical devices fed with a fuel and an oxidant in order to transform chemical to electrical energy. As long as the fuel and oxidant are present in the fuel cell the energy transformation is continuous.

Fuel cells can be divided into six types as shown in table 1.1.

| Type | Electrolyte | Operating temperature (°C) |
|--------------------------|--------------------------------------|----------------------------|
| Alkaline | Potassium hydroxide | 50-90 |
| Proton exchange membrane | Polymeric | 50-125 |
| Direct methanol | Sulphuric acid or polymer | 50-120 |
| Phosphoric acid | Orthophosphoric acid | 190-210 |
| Molten carbonate | Lithium potassium/ carbonate mixture | 530-650 |
| Solid oxide | Stabilized zirconia | 900-1000 |

Table 1.1: The six types of fuel cell

The cleanest and most efficient way to exploit hydrogen is through a fuel cell. More specifically due to their low operational temperature, Proton Exchange Membrane (PEM) fuel cells are seen as the main device to exploit hydrogen. Solid Oxide Fuel Cells can also be used with hydrogen but their high operational temperatures minimize their use to large scale or stationary devices, in contrast to PEM fuel cells which can be used to power a range of different appliances from a mobile phone to a car or a boat.

The operational principle of a PEM hydrogen fuel cell as illustrated in figure 1.2 can be described as follows:

A PEM fuel cell consists of two electrodes (the anode and cathode), an electrolyte between the electrodes made of nafion and catalysts layers of platinum between each electrode, hydrogen and oxygen are fed to the anode and cathode side respectively. The final outcome of the operation is water and electrical energy as a result of the reaction:

1.14

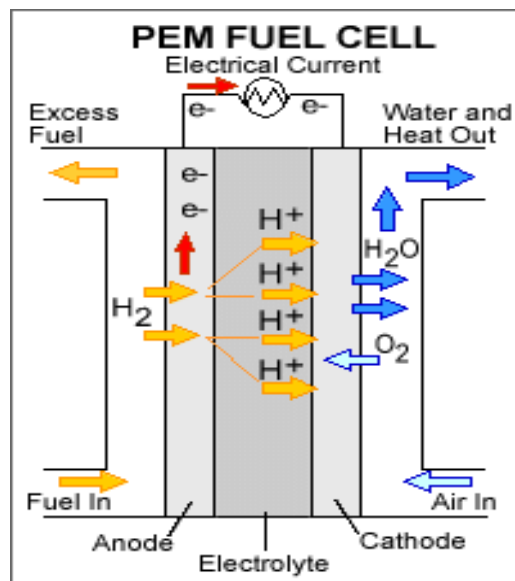
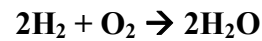


Figure 1.2: Illustration of how a PEM fuel cell works[18] (source: US Department of energy)

A partial reaction takes place at each side of the electrode as described by equations 1.15 and 1.16. At the anode side, hydrogen is oxidized producing electrons and hydrogen ions. Electrons travel to the cathode through an external circuit producing electrical current while the hydrogen ions flow through the electrolyte where they combine with the oxygen to form water at the cathode



In order for a PEM fuel cell to work efficiently and for a long period of time, ultra pure hydrogen is required as contaminations by CO and sulphur can poison the catalyst and electrolyte [19, 20].

1.5 Need for hydrogen purification

During the production of hydrogen from hydrocarbons as mentioned above, a number of other gases as well as some substances such as CO, CO₂, CH₄, H₂O, nitrogen, tar are also produced, making it unattractive for use in fuel cells and other hydrogen related applications mention previously; consequently hydrogen must be separated from these

impurities in order to be usable for energy generation purposes such as fuel cells [2, 5, 21, 22]. The best way to end up with ultra pure hydrogen is by purifying it with the use of dense-metal membranes [5, 8, 21-26].

Chapter 2

Literature Review

2.1 Hydrogen Separation

As previously mentioned PEM fuel cells require ultra pure hydrogen for the best possible operation, but during the production of hydrogen and depending on the method used a mixture of other substances such as: CO, CO₂, N₂, H₂S, NH₃, H₂O and tar are also produced. Therefore the production of ultra pure H₂ requires it to be separated from all the by-products present[2].

The three major ways to the purify hydrogen are pressure-swing adsorption (PSA), cryogenic distillation and membrane separation.

2.1.1 Pressure swing adsorption

Pressure swing adsorption is a mature technology and the most often used in the petrochemical industries. It is based on the property of adsorbent materials to create stronger physical bonds with the impurity molecules at high partial pressure than in

low partial pressures. There are different adsorbents used for different kind of impurities as it can see in the table below.

| Type | Main adsorption duty |
|---------------------------|--|
| Alumina oxides | water |
| Silicagel | water, h.h.c., CO ₂ |
| Activated carbon | CO ₂ , CH ₄ , C ₂ ⁺ , N ₂ |
| Molecular sieve (zeolite) | CH ₄ , CO, N ₂ |
| Carbon mol. sieve | O ₂ |

Table 2.1 : Adsorbent material used in PSA [7]

In a PSA unit, large cylinders with fixed beds of adsorber are used. Thus, at high partial pressure, impurities are adsorbed inside these beds. Impurities are then removed from the system as the pressure decreases. More specifically the PSA process is divided into five steps: 1) Adsorption, 2) concurrent depressurization, 3) countercurrent depressuization, 4) purge, 5) repressurization.

During adsorption, feed gas enters the PSA system at the highest operational pressure. Impurities are trapped inside the adsorber material and high purity hydrogen is removed from the system as the final product. For continuous flow of the feed and the final product, multiple adsorbers are used. Thus feed gas can be driven to a fresh adsorber each time an adsorber is saturated with impurities. Some of the hydrogen is trapped along with the impurities. In order to release it; absorber is depressurized in the second step of the process. During countercurrent depressurization adsorber is partially regenerated by depressurizing leading to the withdrawal of impurities. To further regenerate the adsorber, hydrogen taken from the second step of the process is used to purge it. At the last part of the process

adsorber is repressurized using the hydrogen from the second step and a part of the final product, when needed pressure is reached the adsorption is ready to repeat the cycle.

PSA can produce hydrogen with purities of up to 99.99% with the recovered hydrogen depending on issues like the inlet pressure, purge gas pressure, initial level of impurities and hydrogen concentration in the feed gas. Pure hydrogen produced from this method has a limited pressure below 200 kPa, meaning that further compression is needed for storage in pressurized cylinders. PSA works well at large to medium scale but it is hard to scale it down, while the energy consumption is also high.

2.1.2 Cryogenic distillation

Cryogenic distillation is a low temperature process that uses the different boiling temperatures of the feed gas substances in order to separate them. Hydrogen has a much lower boiling point than the impurities in the feed gas (only He (-268.9°C) has a lower boiling point than H₂ (-252.9°C)) and can be separated from them. But the hydrogen produced is not of very high purity (~99.95%) and thus is a very energy intensive method and works better at large scale.

2.2 Hydrogen separation membranes

In recent years, hydrogen separation membranes have claimed increased interest. While PSA and cryogenic distillation are commercially available and mature techniques, they can typically only be used on a large-scale with high energy demands. On the other hand,

hydrogen-selective membranes are considered to be much less demanding in energy-usage, are relatively easy to produce and handle, and can operate on either a small or large-scale. They do not have any moving parts, and are reliable, while dense metal membranes are also commercially available. Furthermore, they can also be used in membrane reactors where hydrogen production and purification is carried out simultaneously[27]. Due to their hydrogen selectivity membranes can achieve purities of up to 99.999995%, in comparison to 99.99% and 99.95% for PSA and cryogenic distillation respectively. Thus hydrogen selective membranes are considered to be the best solution for the production of ultra pure hydrogen [21].

Hydrogen separation membranes have the ability to allow hydrogen to permeate through them and block almost all other substances. These membranes are divided into porous and dense membranes [5, 21]. Dense membranes can be further separated into polymeric and metallic; porous membranes depending on pore diameter, are separated into microporous and mesoporous while the permeation of hydrogen through a membrane can be based on a number of different mechanisms according to the type of the membrane and the material or materials they consist of [2, 5, 21, 22, 26].

2.2.1 Porous membranes

Porous membranes can be made from a variety of materials such as metals, ceramics and polymer with the common characteristic of a finely controlled pore size.

Usually the pore size is in the range of nm, classifying these membranes as microporous (pore diameter less than 2 nm), the material most often used is ceramic such as Al_2O_3 .

Microporous ceramic membranes operate through a molecular sieving mechanism, which works on a size exclusion principle leaving the smallest molecules components of the gas mixture to pass while blocking the large ones[21].

Being chemically inert, these porous membranes can operate at high temperatures and pressures and with gases such as CO and H_2S that are poisonous to metallic membranes. They also show very high permeation performances while hydrogen flux is directly proportional to pressure. On the other hand they are fragile and because they are porous, purity is limited to ~99% [21].

2.2.2 Dense membranes

Based on the material used dense membranes are separated into polymeric and metallic membranes.

Polymer membranes mainly based on polyamide-imide block co-polymers are used for the separation of hydrogen from substances like nitrogen, carbon monoxide and hydrocarbons. These are cheap to fabricate and operate, they are able to cope with high pressure drops and have low operation temperatures (~373 K) [21, 28]. However, they are sensitive to certain chemicals (e.g. HCl, SO_x , CO_2), to swelling and compaction as they are quite fragile[21, 28]. Hydrogen separation through a polymeric membrane is based on the solution-diffusion mechanism much like the way dense metallic membranes work for hydrogen separation.[5, 21, 26, 28]

Dense metallic membranes are the best choice for the separation of hydrogen that is going to be used on sensitive and demanding applications such as PEM fuel cells, analytical

instruments or used in the semiconductor and aerospace industry. Dense metallic membranes can be made of pure metals like Pd, V, Nb, Ta and Ti or alloys of these metals (e.g. PdAg, PdY, $V_{85}Ni_{15}$, $V_{90}Ti_{10}$, $Ta_{53}Ti_{28}Ni_{19}$, $Nb_{39}Ti_{31}Ni_{30}$)[2, 5, 21]. Dense metallic membranes can operate at high temperatures at which the production of hydrogen usually takes place as in the case of methane steam reformation. Currently the base material most frequently used for the fabrication of dense metallic membranes are Pd-Ag alloys. The permeation of hydrogen through dense metallic membranes is based on the solution-diffusion mechanism.

2.3 Solution-diffusion mechanism

This hydrogen permeation mechanism through a dense metallic membrane can be described as shown in figure 2.2 [1-3, 8, 21, 23-26, 29-32]:

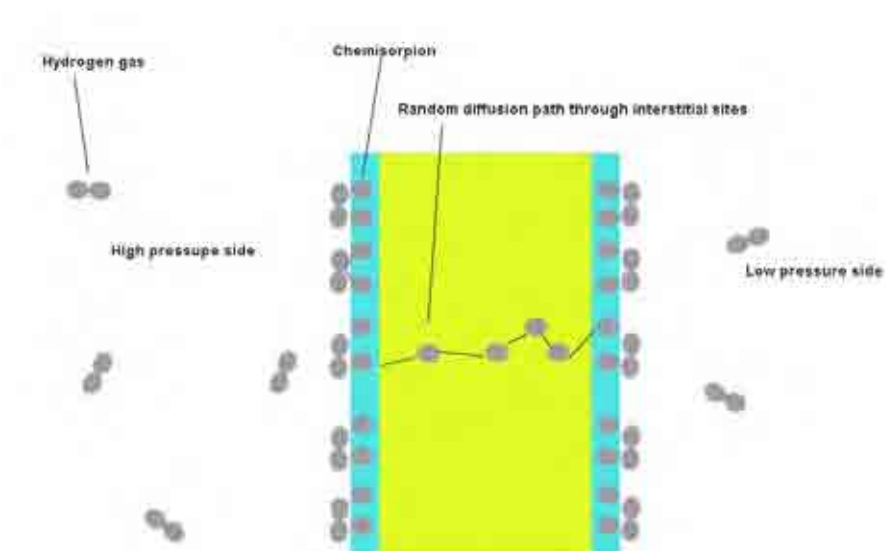


Figure 2.2: Illustration of how a dense metallic membrane works

Hydrogen transportation from one side of a dense metallic membrane to the other can be divided into five steps:

1. On the feed stream side of the membrane, molecular hydrogen adsorbs and dissociates into atomic hydrogen on the metal surface $H_{2(gas)} \rightarrow 2H_{(chemisorbed)}$
2. Absorption of hydrogen into the bulk metal.
3. Diffusion of hydrogen atoms through the interstitial sites of the metal lattice.
4. Transition from the bulk to the near surface region of the membrane.
5. Recombination of the atomic hydrogen and desorption as molecular hydrogen.

The flux of hydrogen through a metal membrane can be quantified in terms of hydrogen permeability $[\Phi]$ which is a product of the diffusivity (D), and the solubility of hydrogen (S) within the metal lattice, as shown in equation 2.1.

$$\Phi = DS$$

2.1

$$[D] \equiv \frac{m^2}{s}, \quad [S] \equiv \frac{mol}{m^3 Pa^{0.5}}, \quad [\Phi] \equiv \frac{mol}{s m Pa^{0.5}}$$

Assuming equilibrium between the external molecular gas phase and the atomic hydrogen phase at the gas/metal interface, the concentration of atomic hydrogen in the first layers of the metal is given by Sieverts' law as being proportional to the square root of partial hydrogen pressure (equation 2.2).

$$C = K_s \sqrt{P}$$

2.2

$$[K_s] = \frac{\text{mol Pa}^{0.5}}{\text{m}^3}, \quad [P] = \text{Pa}$$

Where K_s is Sieverts' constant and P the partial pressure of the applied hydrogen gas phase. Assuming that hydrogen atoms don't interact among themselves during diffusion through the interstitial sites of the lattice and that this atom/membrane system is a dilute solution, Sieverts' constant can describe the solubility of hydrogen atoms inside lattice membrane. The square root appears as a result of the molecular hydrogen dissociating into two hydrogen atoms.

Once hydrogen atoms are inside the metal lattice they diffuse according Ficks' First Law of Diffusion which expresses hydrogen flux (J) as a function of diffusion coefficient and concentration gradient (equation 2.3).

$$J = -D \frac{dC}{dx}$$

2.3

$$[C] = \frac{\text{mol}}{\text{m}^3}$$

With x being the membrane thickness and C the hydrogen concentration.

Now if we combine Sieverts' law with Ficks' first law we have:

$$J = -D \frac{d}{dx}(K_S \sqrt{P}) \Rightarrow J \int_1^2 dx = -DK_S \int_1^2 d\sqrt{P} \Rightarrow$$

$$J(x_2 - x_1) = -DK_S(P_2^{0.5} - P_1^{0.5}) \Rightarrow Jx = DK_S(P_1^{0.5} - P_2^{0.5}) \Rightarrow$$

$$\Rightarrow J = \frac{DK_S(P_1^{0.5} - P_2^{0.5})}{x}$$

$$DK_S = \Phi$$

So the flux of hydrogen through a dense metallic membrane is given by the equation 2.4

$$J = \Phi \frac{[P_1^{0.5} - P_2^{0.5}]}{x}$$

2.4

$$[J] = \frac{\text{mol}}{\text{m}^2\text{s}}$$

Here P_1 and P_2 describe the feed and permeation side of the membrane respectively.

Because 0.5 dependency is not always found in practice, Equation 2.4 can be change to as

$$J = \Phi \frac{[P_1^n - P_2^n]}{x}$$
 where n varies from 0.5 to 1 .The main reason for deviations from Sieverts'

law has to do with the conditions on the surface, these conditions may have to do either with the surface itself or with insufficient pressure and temperature conditions over it with n increasing towards 1 when permeation is limited by surface adsorption and desorption steps.

The surface of a membrane is very important as the dissociation of molecular hydrogen takes place here, allowing atomic hydrogen to diffuse into the metal. An active and high surface area can decrease the activation energy of the dissociation and recombination of hydrogen thus making the whole solution-diffusion permeation mechanism effective and less energy costly. The more active a surface is, the higher the flux and permeability properties of the hydrogen separation membrane.

Extensive contamination on the surface, inactive, or not sufficiently active surfaces can increase the activation energy to a point where solution-diffusion is not the dominant mechanism. Low temperatures and partial pressures can also hinder the dissociation and recombination reactions even at an active surface leading, again to deviations from the square root dependency.

Another common reason for the deviation from the 0.5 dependency derives from the introduction of other permeation mechanisms along with solution-diffusion, for example molecular hydrogen diffusion through grain boundaries or via surface diffusion in membranes that are not 100% dense, will lead the 0.5 power law dependency to be increased towards 1.

The activation energy (E) for permeability can be calculated through the Arrhenius type equation, 2.5

$$\Phi = K_s \exp\left(-\frac{E}{RT}\right) \quad 2.5$$

Where R and T are the gas constant and absolute temperature respectively

$$[E] \equiv \frac{J}{mol}, \quad [T] = K, \quad R = 8.314 \frac{J}{mol * K}$$

When $n = 0.5$ the rate limiting step in permeation is diffusion, also diffusion and solubility have an Arrhenius relationship with temperature thus equation 2.5 will be valid only when $n = 0.5$. Activation energy of permeation is the sum of diffusion and adsorption/desorption activation energies.

2.4 Palladium-based membranes

Palladium is a Group 10 transition metal that has the ability for almost perfect hydrogen selectivity; it also has high hydrogen solubility and diffusivity properties as well as a high

ability to disassociate molecular hydrogen into its atomic state. For these properties, palladium is highly desirable as the base material for the fabrication of hydrogen separation membranes; palladium alloys based membranes can produce hydrogen of just a few ppb impurity levels, perfect for the use in PEM fuel cells.

However, palladium is a very expensive commodity; in addition, when exposed to hydrogen under certain conditions it can become very brittle, due to β -hydride formation. These drawbacks prevent the use of palladium being established in a future hydrogen economy, at least not at an extensive commercial level.

Alloying Pd as well as fabricating composite membranes where the amount of palladium is minimized, are the two ways that are currently being used to resolve these problems with Pd.

In the presence of hydrogen below 300°C and 20.15×10^5 Pa, Pd experiences a $\alpha \rightarrow \beta$ phase transition that leads to mechanical instability known as hydrogen embrittlement [4]. Hydrogen diffuses interstitially by taking up octahedral sites through the face centered cubic (fcc) lattice structure of palladium, causing it to create a new phase. For concentrations up to $\text{PdH}_{0.02}$ at RT, α -phase occurs, for concentration above that, β -phase is created which is immiscible with α -phase thus creating a miscibility gap. Because β -phase has a larger lattice constant and consequently considerably expanded lattice compared to the α -phase, the existence of both leads to warping and embrittlement of the membrane. When hydrogen in the system reaches over 60 at. % α -phase no longer exists and β -phase is the only one present.

This mechanical integrity problem can be solved by decreasing the critical temperature of the phase transition. To do so Pd is alloyed with other metals such as silver (Ag), copper

(Cu) and yttrium(Y). The most common Pd alloy used commercially today for hydrogen purification is Pd-25Ag[8].

The obvious way to reduce the cost of Pd-based membranes is to reduce the amount of Pd used in them, without losing the efficiency and mechanical stability that typical Pd based membranes have in the process of hydrogen separation for high end applications. Thus thin Pd or Pd alloys films ($< 20 \mu\text{m}$) can be the base of efficient, cheap Pd based membranes when combined with a porous material support.

The porous material will provide the membrane with the necessary mechanical stability without adversely affecting hydrogen flux thus very thin Pd based films can be deposited on top of porous substrates minimizing the use and ultimately the cost of Pd. The thickness of the Pd layer mainly depends on the pore diameter and the smoothness of the substrate surface. Substrates with small pores and smooth surface require smaller quantities of Pd in order for a dense, defect free film to be formed on top of them. Stainless steel or ceramic materials are the most common choices for use as substrates.

Issues like the porosity, roughness of the support surface and different crystallography between the support and palladium film make the fabrication of composite membranes a hard and delicate procedure. Methods like Electroless plating, Physical Vapor Deposition and Chemical Vapor Deposition are usually used in the production of composite membranes[8].

Currently composite membranes produced have shown a number of stability issues as well as a loss of permselectivity towards hydrogen for increased temperatures, also the deposition of palladium using the methods previously mentioned will create films with unstable microstructure. Thus microstructural changes are possible to occur at high temperatures[8].

2.5 Novel materials for the fabrication of dense metallic membranes

Refractory materials of subgroup VB such as vanadium (V) niobium (Nb) and tantalum (Ta) have higher hydrogen permeability compared to other metals used on hydrogen selective membranes as can be seen in Figure 2.4, making them possible candidates to replace palladium as the base material for the fabrication of high efficiency and cheap hydrogen purification membranes.

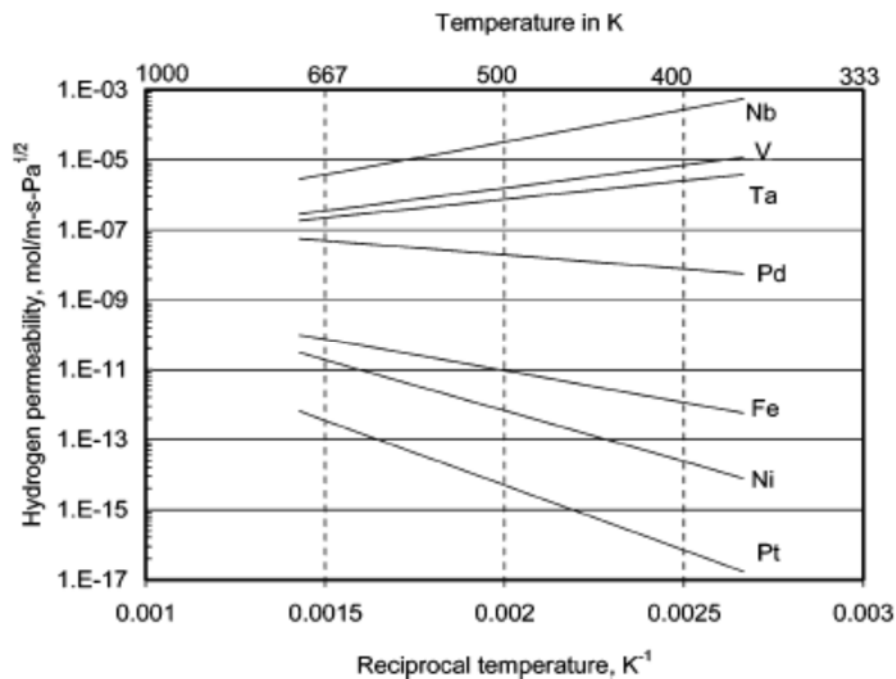


Figure 2.4: Hydrogen permeability of V and Nb can be two and four order of magnitude higher than Pd respectively (the data for Nb, V, Ta and Pd weren't direct measured but calculated from solubility and diffusion measurements) [21, 33]

However, the interaction of these metals with hydrogen is less energetic due to their inactive surface. Thus the flux is rate limited by the dissociation and absorption reactions of hydrogen, leading to deviation from Sieverts' law and ultimately to lower hydrogen flux and permeability making them unattractive for use as hydrogen separation membranes [1-3, 34].

In 1967 Makrides et al. [2, 3] first managed to overcome the surface effects of refractory metals by first cleaning, and then vapor-depositing Pd on the two sides of the potential membrane. By using the highly catalytic Pd Makrides et al. was able to activate the membrane surfaces allowing the hydrogen dissociation and recombination reactions [2, 3]. After the dissociation of hydrogen the Pd surface and chemisorption of the atomic hydrogen through the Pd layer, atomic hydrogen can diffuse through the refractory metal much faster. This is a result of the lattice structure of vanadium and niobium being body centered cubic (bcc), a structure much more open than the face centered cubic (fcc) structure of Pd.

The higher hydrogen solubility and bulk diffusion that take place at lower activation energies are the main properties that result in vanadium and niobium being much more permeable than palladium [table 2.2]. Conversely vanadium and niobium form hydrides much more readily than Pd as the formation reactions are both exothermic (negative enthalpy) and energy will be released in the form of heat [1, 2, 29, 32, 34, 35].

These composite membranes are now the main focus of research as they seem to have the potentials to reach performance targets that organizations such as The USA Department of Energy have set [21][table 2.3]. Improvements in properties and techniques such as the coating method, durability and overall flux are under way in order for them to replace Pd as the core elements of dense metallic membrane.

| | Crystal structure | Hydride formation enthalpy (kJ/mol) | H ₂ permeability at 500°C (mol/m*s*Pa ^{0.5}) | Activation energy for bulk diffusion of hydrogen (kJ/mol) |
|----|-------------------|--|--|--|
| Nb | bcc | -60(NbH ₂) | 1.6* 10 ⁻⁶ | 10.2 |
| V | bcc | -54(VH ₂) | 1.9* 10 ⁻⁷ | 5.6 |
| Pd | fcc | 20(PdH ₂) | 1.9*10 ⁻⁸ | 24.0 |

Table 2.2 : Nb and V properties in comparison to Pd when interact with hydrogen [2]

| Characteristic | 2003 status | 2010 target | 2015 target |
|---|-------------|-------------|-------------|
| flux rate (m ³ /h/m ²) | 18.3 | 61 | 91.5 |
| Cost(\$/m ²) | 1940 | 1080 | <1080 |
| Durability (years) | <1 | 3 | >5 |
| Operating temperature (°C) | 300-600 | 300-600 | 250-500 |
| Operating ΔP (MPa) | 0.69 | <2.76 | 2.76-6.89 |
| Hydrogen purity | >99.9 | >99.95 | 99.99 |

Table 2.3: Metallic membranes for hydrogen separation targets [2]

2.5.1 Niobium hydrogen and Vanadium hydrogen systems

Both V and Niobium are metals with a bcc lattice structure. In bcc metals hydrogen diffuses through the tetrahedral interstitial sites. It has been found that in general the distance between two neighbouring tetrahedral interstitial sites for a bcc metal is two times smaller in comparison to the analogous octahedral distance for an fcc metal. As a result hydrogen atoms will diffuse from one site to the other faster, thus resulting in hydrogen diffusion through a bcc metal to be characterized by much higher values of diffusion coefficients and lower activation energies [2, 21, 23, 32].

When hydrogen is absorbed by Niobium a number of phases are created. For temperatures above 171 °C bcc solid solution phases α (Nb) and α' (Nb) are formed at low and high hydrogen concentrations respectively with the lattice parameters being proportional to hydrogen concentration expressed by:

$$\frac{\Delta\alpha}{\alpha} = (4.72 \pm 0.25) \cdot 10^{-4} / \% \frac{H}{Nb} \quad 2.6$$

For temperatures lower than 171°C a number of non bcc phases are created while for very high hydrogen concentrations, the system is transformed into an fcc structure that is very

fragile and has a NbH₂ composition. In this phase the hydrogen atoms will occupy tetrahedral sites[35].

Similar to Niobium, when H is absorbed by V, disordered and ordered interstitial solid solution phases are formed. For temperatures above 220 °C α (V) and α' (V) bcc disordered solid solution phases are formed at low and high concentrations respectively with the lattice parameters being expressed as

$$\frac{\Delta\alpha}{\alpha} = (5.73 \pm 0.3) \cdot 10^{-4} / \% \frac{H}{V} \quad 2.7$$

Below 220 °C a number of different phases are created depending on hydrogen composition. Thus for compositions above 33.3 at. % and up to 50 at.% V₂H or β phase is created while dihydride phase VH₂ is formed above 66.7at.% with an fcc structure and tetrahedral interstitial sites[35]. It must be noted that the vanadium-deuteride system (V-D) is distinctively different from the V-H system [35].

2.6 Literature Review summary

Pd-Ag alloys based membranes are commercially used to remove hydrogen from the mix of gases produced during the different methods of hydrogen production with the most significant being the reformation of natural gas. These types of dense metallic membranes can produce hydrogen of extra high purity of up to 99.999995% also in comparison to other commercial methods of hydrogen purification like pressure swing absorption and cryogenic

distillation, not only produce hydrogen of higher purity but are easy to produce and operate, while have very low energy needs and scalable properties.

The cost of palladium has created the need for search for alternative materials that will be able to replace palladium as the basic element or minimize its use in a hydrogen separation membrane. Literature suggests that refractory metals such as vanadium, niobium and tantalum have hydrogen permeability properties higher than palladium while being much cheaper [1-3, 24, 28, 33].

Vanadium and niobium may have higher hydrogen permeability properties in comparison to palladium but their surface is very inactive. Thus permeation is limited by surface adsorption and desorption steps. Combining these metals with very thin layers of palladium films we can fabricate composite membranes that have increased hydrogen permeability properties and active surfaces with the minimal use of palladium.

2.7 Project aims

The main aim of this project is the utilization of vanadium and niobium metal as dense metallic membranes for hydrogen purification. To do so vanadium and niobium films will be deposited with thin coatings of palladium and then tested with hydrogen in order to verify the hypothesis that palladium will activate their surface and that these membranes can give high values of hydrogen permeability, as well as how well can they tolerate over high temperatures.

A secondary aim of the project will be to test the ability of vanadium as an intermetallic barrier between a SS-Pd couple at temperatures where palladium will diffuse into stainless steel. Due to vanadium having a higher melting point than palladium it can potentially block the effect of palladium diffusion into stainless steel.

Chapter 3

Experimental Approach

3.1 Preparation of Pd Coated V and Nb Foils

Vanadium (99.8+ %) and Niobium (99.9%) light-tight foils were purchased from Goodfellow company, both foils measured 10x10 cm, with a thickness of 25 μm . “Light tight” is the term used by this company to describe foils that are pinhole free. Thus by selecting this type of foil, the membranes were guaranteed to be fully dense.

From these foils 18 mm diameter disks were cut to be coated with a Pd layer and later tested in the hydrogen permeability apparatus. Prior to the Pd coating process the disks were treated to remove any surface oxide, which could adversely affect the properties of the membrane. Under an argon atmosphere, both sides of the discs were abraded using 800 grit size SiC paper followed by cleaning with IMS.

3.2 Preparation of stainless steel (SS) discs

Stainless steel disks (316 type) with a 1 cm diameter and 0.25 mm thickness were purchased from Goodfellow Company in order to fabricate SS–Pd, SS-V-Pd and SS-V diffusion couples. Prior to the deposition of the palladium or vanadium films, the disks were cleaned with IMS.

3.3 Coating Process

A Closed Field Unbalanced Magnetron Sputter Ion Plating system (CFUBMSIP) produced by Teer Coatings Ltd was used for the deposition of thin and cohesive layers of Pd and V on top of V, Niobium and stainless steel substrates. The magnetrons are arranged such that at least one pair is of opposite polarity as illustrated in figure 3.1. This configuration traps the plasma, thus preventing the escape of ionizing electrons.

The system consists of a stainless steel chamber in which, with the assistance of a diffusion pump, high vacuum can be produced in order for the operation to take place. The substrates are loaded on a rotating sample holder at the centre of the chamber. When the vacuum inside the chamber is below 10^{-6} mbar, a controlled flow of argon gas is emitted, with the vacuum pumps still running, raising the pressure in the system to the level required to operate the magnetrons ($\sim 10^{-3}$ mbar). A magnetron is the basic unit of the sputtering system; it consists of the target (a plate of material of which the coating is to consist of) with a

magnet behind it in order to create a magnetic trap for charged particles, such as argon ions, in front of the target.

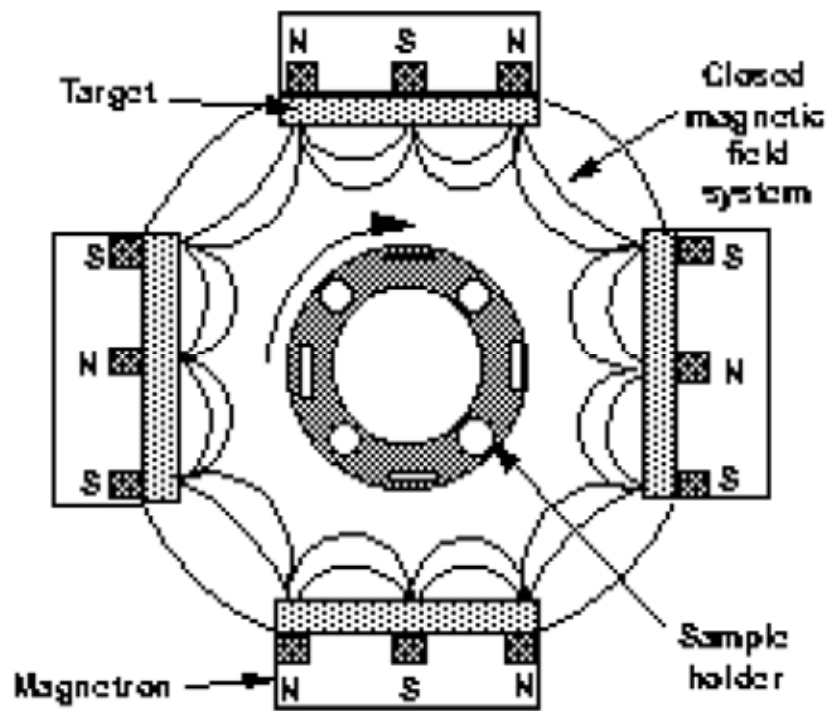


Figure 3.1: The chamber of the magnetron sputtering system[36]

Applying a negative voltage (typically -300V or more) results in the argon ions being attracted to the target surface. When the argon ions hit the surface of the target two processes take place:

- atoms leave the target and as they are neutral charged leave the magnetic trap and form a coating on the substrates, removing atoms in this way is called sputtering.

- during sputtering process the target also produce electrons which are held within the magnetic trap and are used for the ionization of argon so the procedure is continuous.

As heat is also produced using this method, water passes through the magnetrons in order to cool them down. The system at The University of Birmingham consists of four magnetrons thus multilayer films could be produced without the need for target changing.

The system can also clean the substrate prior to coating in the same way.

Cleaning the surface consists of sputtering contaminants from the surface of the sample by ion bombardment. A high negative voltage bias is applied to the samples and a low current is applied to the magnetrons under an argon atmosphere ($\sim 1 \times 10^{-3}$ mbar); under these conditions the main source of ionisation is the magnetron discharge and the function of the sample bias is to draw ions out of the magnetron discharge and accelerate ions to the samples. During the ion cleaning stage the surface of the sample is cleaned of all contaminants and oxide films the surface is also etched off due to the ion bombardment.

The whole process is controlled through the system software; a recipe is written for the whole process and controls all parameters (argon flow, chamber pressure, magnetron current, sample bias voltage and coating time)

Vanadium and niobium foils coated with Pd (Pd-V-Pd, Pd-Nb-Pd), as well as stainless steel couples with Pd (SS-Pd), V (SS-V) and with both vanadium and paladium (SS-V-Pd) were produced. All samples were loaded into the sputtering chamber with the use of an argon glove box attachment on the system thus avoiding the contamination of air sensitive materials. The thicknesses of the films created were 100 and 200 nm as described below.

- Two different types of Pd-V-Pd and Pd-Nb-Pd samples were created, one with 100 nm and one with 200 nm of Pd deposited on each side of the foils. For both thicknesses of Pd the conditions of deposition were the same with the exception of coating time, thus in order to deposit 200 nm Pd the deposition time was double. - 200 V and 1 A was applied to the Pd magnetron the flow of argon was 25 sccm and the coating time was 240s for 100nm Pd and 480 s for 200nm Pd.
- Five different types of SS couples were created using the sputtering system: ss-Pd with 100 nm and 200 nm of Pd deposited, ss-V with 100 nm of V deposited, ss-V-Pd with 100 nm of V followed by 100 nm of Pd deposited and ss-V-Pd with 100 nm V followed by 200 nm of Pd deposited. The conditions used to sputter the Pd were the same as mentioned in the case of the V and Niobium foils, the conditions for V sputtering were 2 A and -200 V applied to the V magnetron the flow of argon was 25 sccm and the coating time was 240 s.
- In order to determinate the coating time needed for the required thickness, glass slides masked with kapton tape were loaded these glass slides were also used during the coating of the samples in order to confirm the exact thickness .

3.4 Confocal laser microscope

A Confocal scanning laser microscope uses a laser beam to scan the specimen in the x-y directions while the light that the detector captures to create the picture passes through a pinhole positioned in such a way so as to allow light only from the focal point to pass through it [figure 3.2]. As a result of this geometry the final pictures are much clearer than when compared to a normal microscope. As only one point is illuminated the image needs

to be scanned over a regular raster. This system can acquire both 2d and 3d images of magnifications up to 100x, making specimen geometries such as height differences easy to measure

An Olympus LEXT OLS 3100 Confocal laser microscope was used to verify the thickness of the deposited films as well as to investigate the surface of deposited films. Films thicknesses were measured using the masked glass slides that were coated along with the samples, the tape was then removed and the height difference between the glass slide and the film were measured (z error of ± 10 nm).

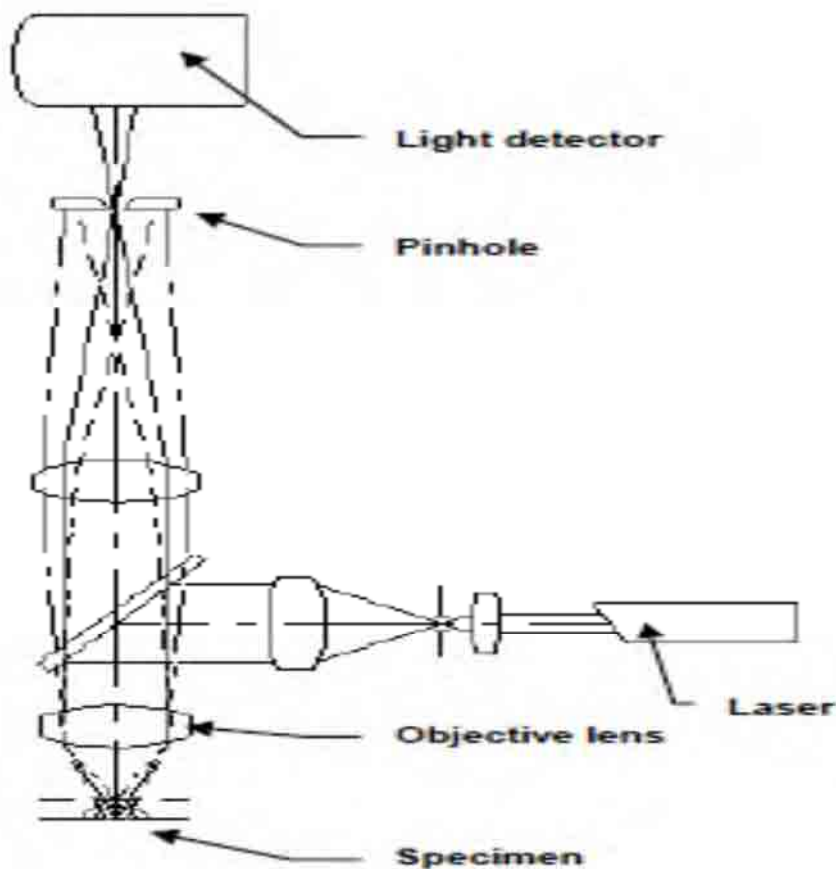


Figure 3.2: Geometry of a Con-focal laser scanning microscope[37]

3.5 Scanning Electron Microscopy (SEM)

Scanning electron microscopy uses electrons instead of light to scan a specimen for images of much higher magnification than normal microscopes can produce. A Jeol 6060 scanning electron microscope was used to study the microstructures of the deposited films; energy dispersive spectrum (EDS) was also used to investigate the composition of the films. When electrons hit the surface of the sample characteristic X-rays are emitted from it as a result of the interaction, EDS uses a detector in order to analyse these X-rays and give us information about the composition of the specific area the X-rays came from. Samples were mounted into the sample holder inside a vacuum chamber.

3.6 Material characterization

A Bruker D8 Advance X-ray diffractometer (figure 3.3) was used for the investigation of the structures and lattices parameters of the Pd-V-Pd, Pd-Nb-Pd and stainless steel couple samples. In-situ measurements at high temperature and pressure were performed using an Anton Paar XKR900 cell; allowing the sample to be heated to temperatures up to 750°C

under a helium or hydrogen atmosphere of pressures up to 1000 kPa and measurements to be performed various temperature intervals.

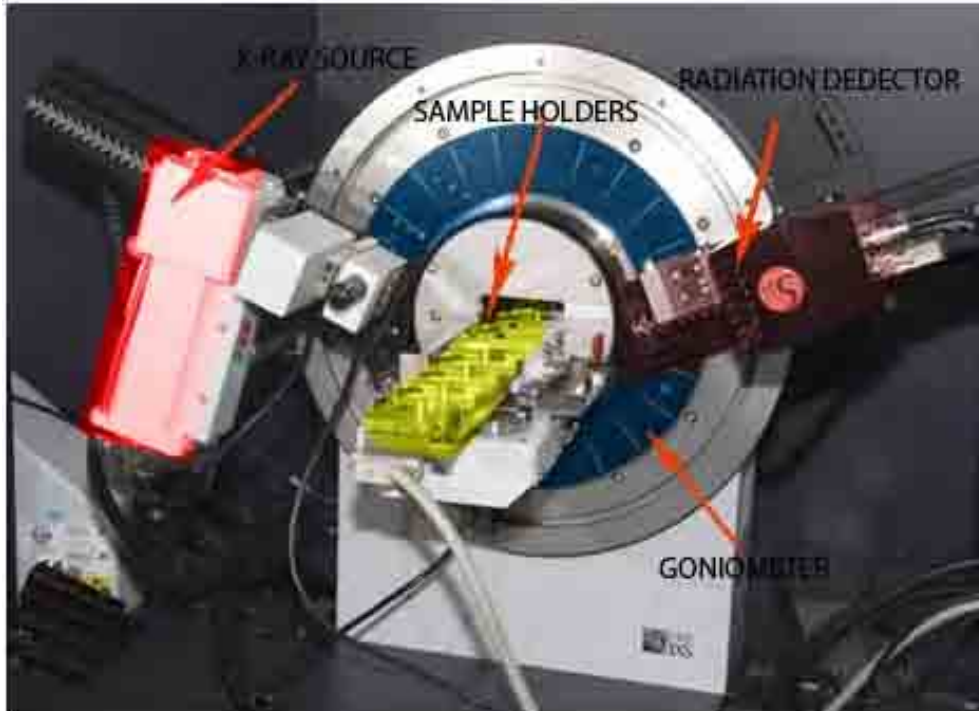


Figure 3.3: D8 diffractometer[38]

When electromagnetic radiation hits a crystal material at certain angles and at certain crystallographic planes, radiation will be enhanced, leading to the phenomenon known as diffraction. Depending on material structure a different diffraction pattern is created.

This x-ray diffractometry process is used for the identification of a material. The angles at which radiation will have constructive interference and create a peak can be found using Bragg equation:

$$\lambda=2d_{hkl}\sin(\theta) \quad 3.1$$

Where λ is the wavelength of the X-ray radiation, d_{hkl} the interplanar spacing and θ is half the angle between the diffraction beam and the original beam, both wavelength and spacing are at the same order of magnitude around ~ 1 Å. The radiation used during this work was $\text{CuK}_{\alpha 1}$, which has a wavelength of 1.54056 Å. The interplanar spacing (d_{hkl}) is related to the lattice parameter (a) of a material using the equation:

$$1/d_{hkl} = a/(h^2+k^2+l^2)^{1/2} \quad 3.2$$

Where a is the lattice parameter.

3.7 Hydrogen permeability apparatus

The apparatus shown in the Figure 3.4 was used for the calculation of hydrogen flux and permeability of the tested membrane. This system applies a controlled feed gas to the high-pressure side of the sealed membrane and monitors the gas that permeates through the membrane on the downstream side at fixed pressures (build-in error of ± 0.005 bar). The hydrogen rate through the membrane is measured using a mass flow controller (± 2 ml/min). Because the mass flow controller hasn't been calibrated for hydrogen a correction factor (1.008*1.045) was used for accurate hydrogen flow data. The flow data can then be used to calculate hydrogen and permeability using the following equations. As it can be seen in Figure 3.4 a number of different gases can be used with the apparatus.

Flux is the flow per area thus $J = \text{flow}/(\text{membrane area})$ while permeability can be calculated using equation 2.4.

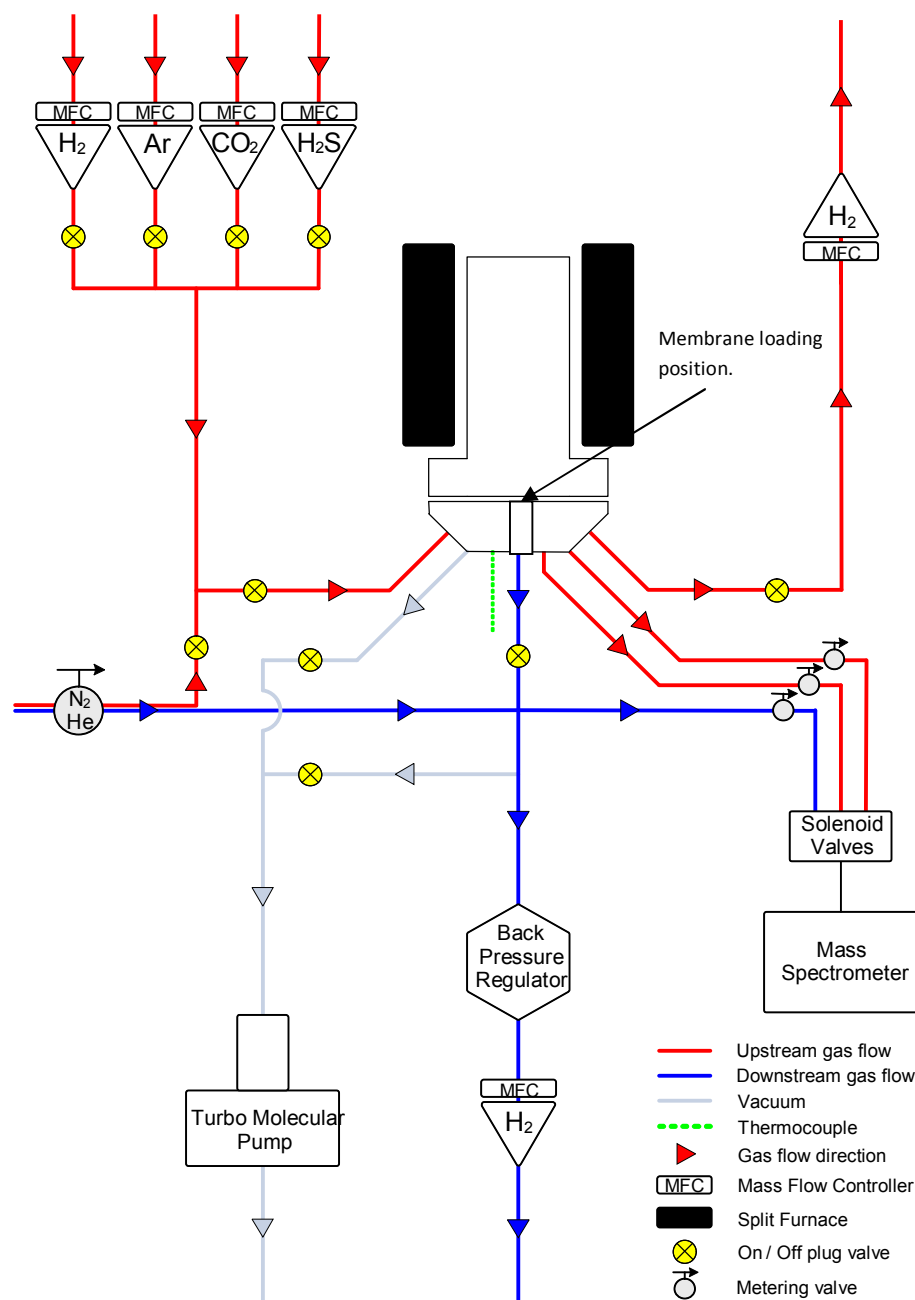


Figure 3.4: Hydrogen permeability apparatus (the diagram was kindly offered by Sean Fletcher)

The membrane is loaded between a knife edge seal and a copper gasket to achieve a leak free seal; the whole system was then sealed with the Inconel furnace tube that fits a split furnace, the temperature of the furnace is measured with a K type thermocouple (build in error of $\pm 0.0015 \cdot (T)$).

After the sample has been loaded a leak test is performed; first vacuum is used to make sure that the system is clean then the system is first left open and a neutral gas like argon or nitrogen is admitted, then a small pressure is allowed to build up on the upstream side of the membrane while the rest of system is isolated by closing all gas inlet and outlets, when the upstream pressure is build up (3 bar) the downstream pressure is checked, if an increase is not observed no leak is present, otherwise the sample is reinstalled and the leak test is repeated.

Because of phase transitions that V and Niobium experience at temperatures below 220°C as mention in 2.5.1 (and because Pd also suffers from a α to β phase transition below 300°C) the membranes were first heated under an argon or nitrogen atmosphere until reaching 300°C. When this temperature is reached the gas is vented and a vacuum is used to clean the system. After that, hydrogen can introduced to the system. After hydrogen is introduced, a combination of isothermal and isobaric measurements was performed.

- Isothermal measurements: The system was left at a stable temperature while the partial pressure ΔP was changed allowing time for equilibrium to be reached before setting the next pressure step. Thus we can take flow data for different pressures at a stable temperature. Using equation (2.4) the isothermic data can be used to plot hydrogen flux against a number of hypothetical ΔP^n including $n=0.5$ (for which Sieverts' law applies), these plots can then be linearly fitted and the coefficient of determination $\langle R^2 \rangle$ is calculated. R^2 represent the percentage of the data that is the closest to the line of best fit. This fit (R^2 closest to one) gives the true value of n and indicates if Sieverts' law is valid or not for the Pd-V-Pd and Pd-Nb-Pd membranes at that temperature.

Also by plotting R^2 vs n we can validate what n value give us the best data fit.

The partial pressures used for these measurements were in the range of 1-0.5 bar with 0.1 bar steps. Measurements were repeated at the different temperatures of the isobaric measurements stated below. Thus validation of Sieverts' law at different temperatures is possible. More specifically the membrane temperatures used were the starting temperature of the operation 330°C, the maximum temperature 450°C and again 330°C during the cooling path from 450°C .

- Isobaric measurements: After 1-0.5 bar pressure range isotherm measurement the pressure is kept at 0.5 bar and the temperature is raised at 2°C/min to 450°C. At 450°C the isotherm measurement is repeated. The system then returns to the first temperature of the isotherm measurement (330°C) again at $\Delta P = 0.5$ bar and same temperature step (2°C/min). Using the isobaric data and equations (2.4) and (2.5) hydrogen flux, permeability and the activation energy of hydrogen dissociation that leads to its diffusion through the membrane can be found.
- Stability measurements: In order to check if the membranes fabricated are stable, they have to keep the same flux properties for a long period of time. Thus measurement at a stable temperature and pressure for a period of time was also executed in order to investigate how stable Pd-V-Pd and Pd-Nb-Pd membranes are. More specifically they were kept at 390°C and ΔP of 0.5 bar for 21 hours and 32 seconds.

All the temperatures mentioned above are referring to temperatures that the membrane has.

Chapter 4

Results and Discussion

4.1 Pd-V-Pd

4.1.1 Material characterization

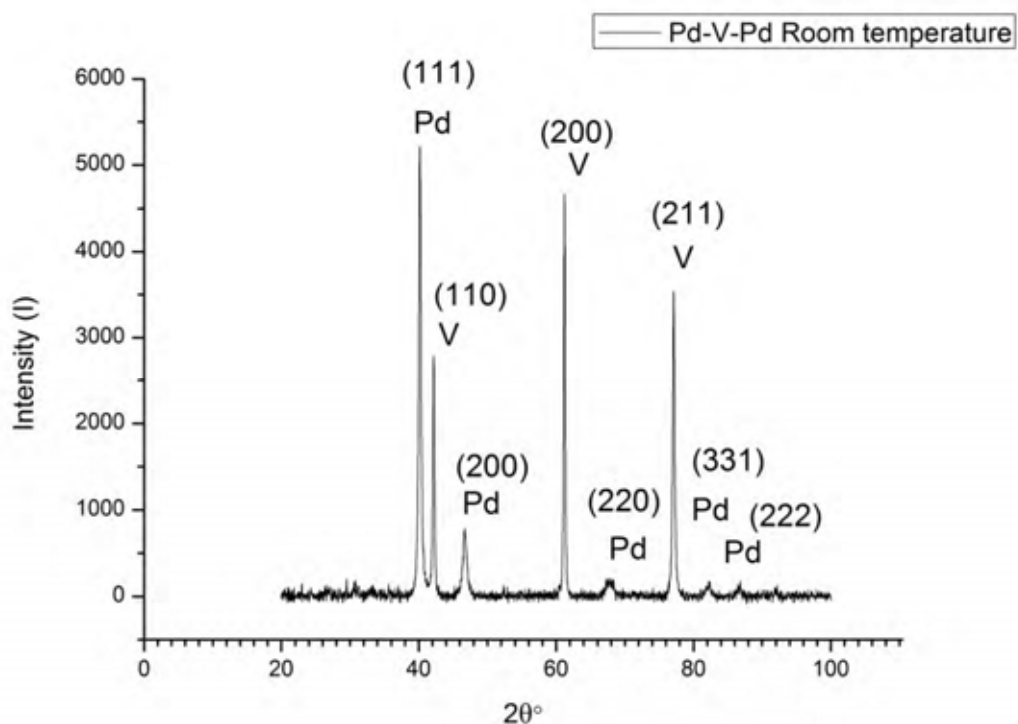


Figure 4.1: XRD pattern of the Pd-V-Pd with palladium thickness of 100 nm fabricated membrane

The XRD pattern in Figure 4.1 confirms that the fabricated membrane consists of Pd and V, using equations 3.1 and 3.2 for each of the pattern peak the mean lattice parameter a is $3.89 \text{ \AA} \pm 0.01 \text{ \AA}$ for Pd lattice and $3.03 \text{ \AA} \pm 0.01 \text{ \AA}$ for V, data that agree with theory.

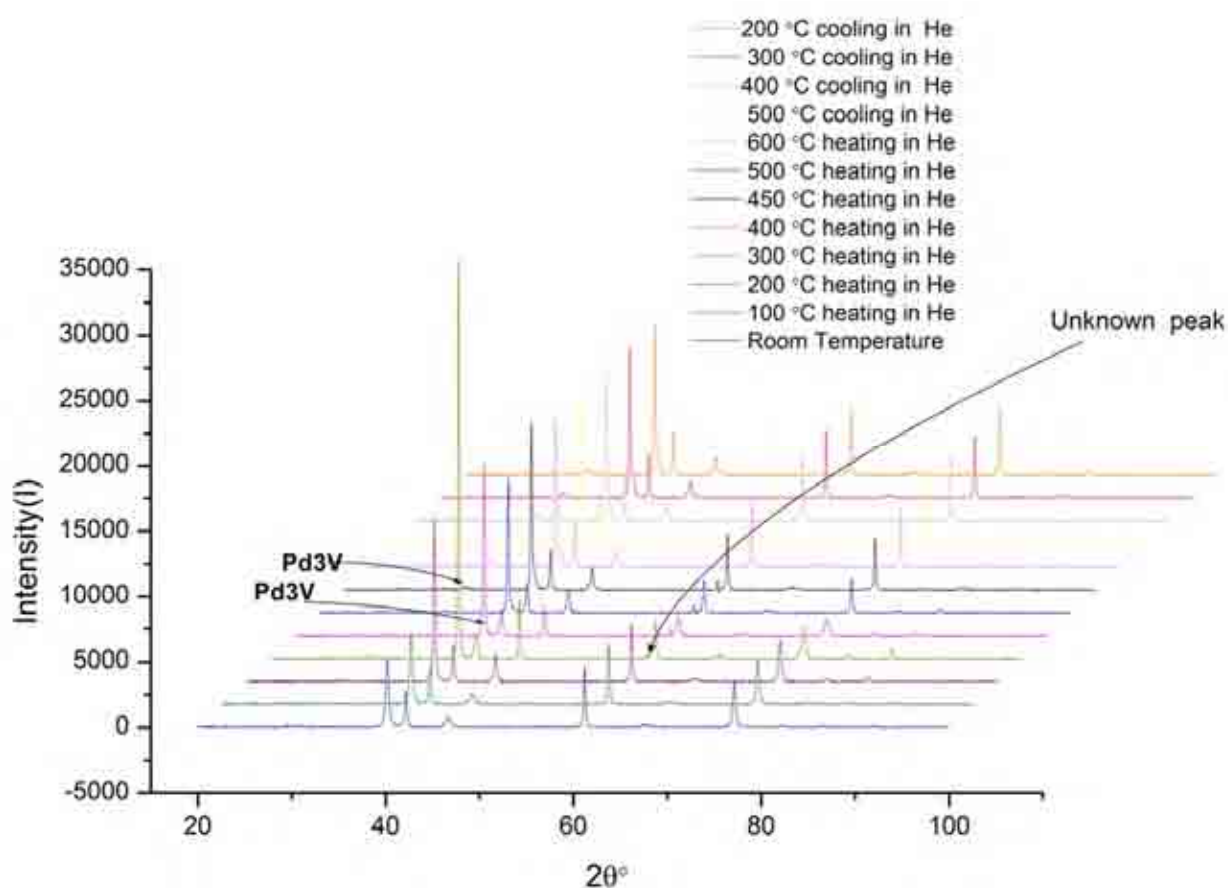


Figure 4.2: Pd-V-Pd membrane XRD pattern at 0.5 bar partial pressure of Helium at different temperatures.

At temperatures above 400 °C the creation of palladium vanadium alloys starts to occur. At 400°C a peak at 2θ 40.44° is created while at 500 a new peak is also created at 32.98 °, these two peaks that start to emerge at these temperatures increase in intensity as the temperature goes up while they remain stable during cooling at 200°C. The creation of those two peaks indicate the creation of Pd3V. An unknown peak is created at 59.92 ° from 300°C until

600°C while it disappears during cooling. The origin of this peak is due to contamination on the Anton Parr cell window and can be discounted.

The creation of this alloy part of the diffusion of Pd inside V at elevated temperatures can cause hydrogen permeability to be decreased, a phenomenon previously described in literature by David J. Edlund et al. [39].

As expected, temperature causes the lattices of V and Pd to expand, as the main peaks shown in Figure 4.2 are shifted to the left as temperature increases.

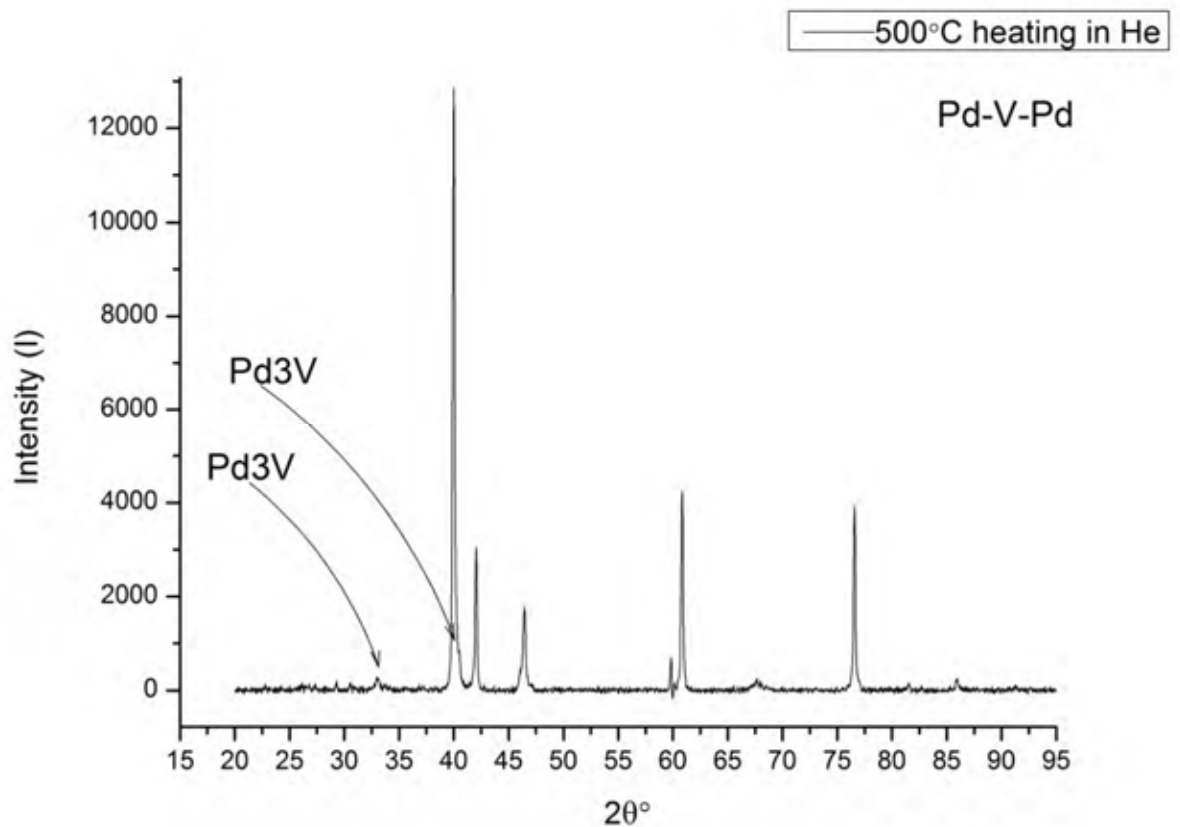


Figure 4.3: XRD pattern of Pd-V-Pd at 500 °C in the presence of He here the peaks mention above can be seen better.

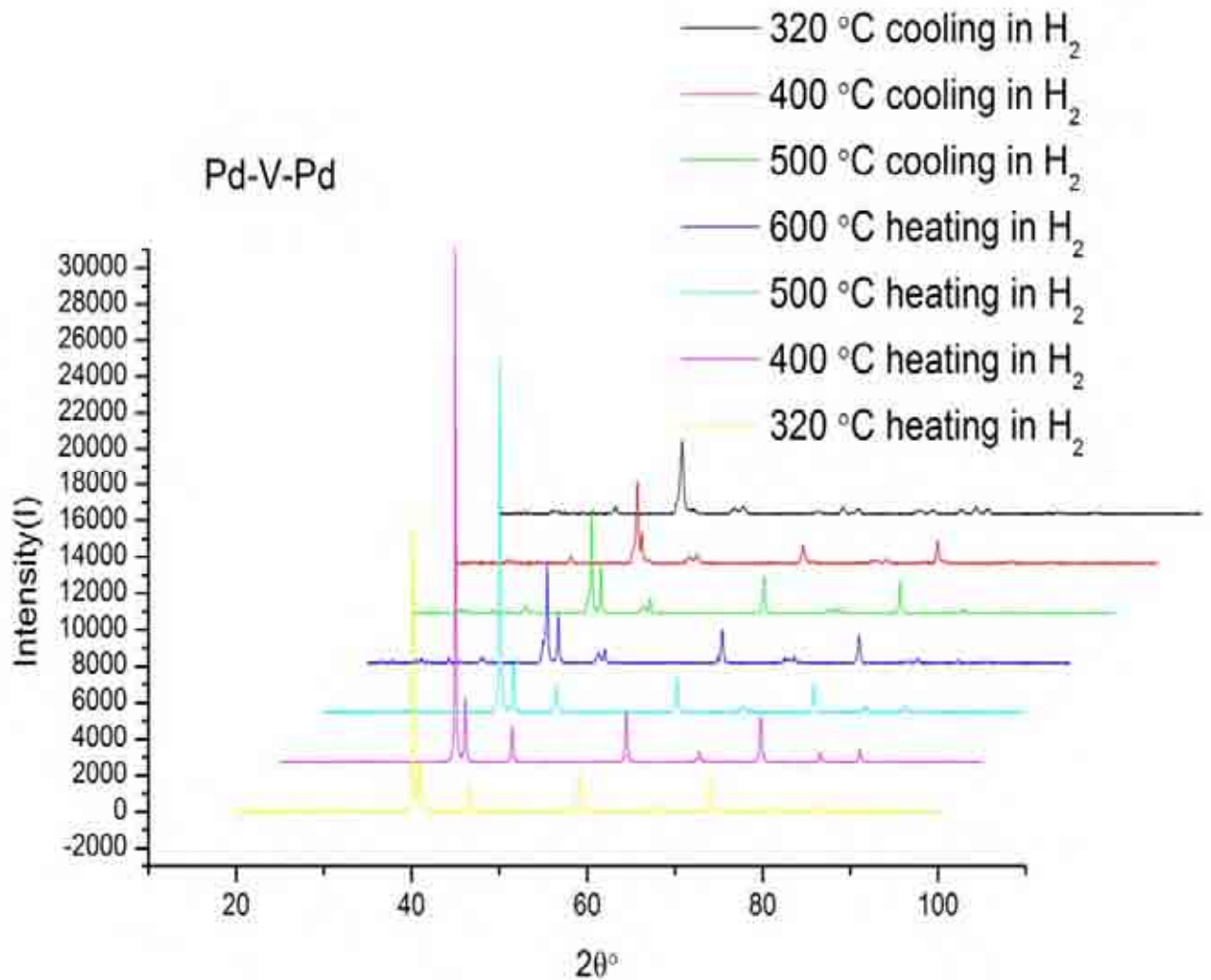


Figure 4.4: The XRD pattern of Pd-V-Pd at 0.5 partial pressure of hydrogen at different temperatures.

The use of hydrogen will increase the phenomena described above. As it can be better seen in figure 4.5 the presence of hydrogen affects vanadium much more in comparison to palladium as the main peaks of V are extensively shifted to the left.

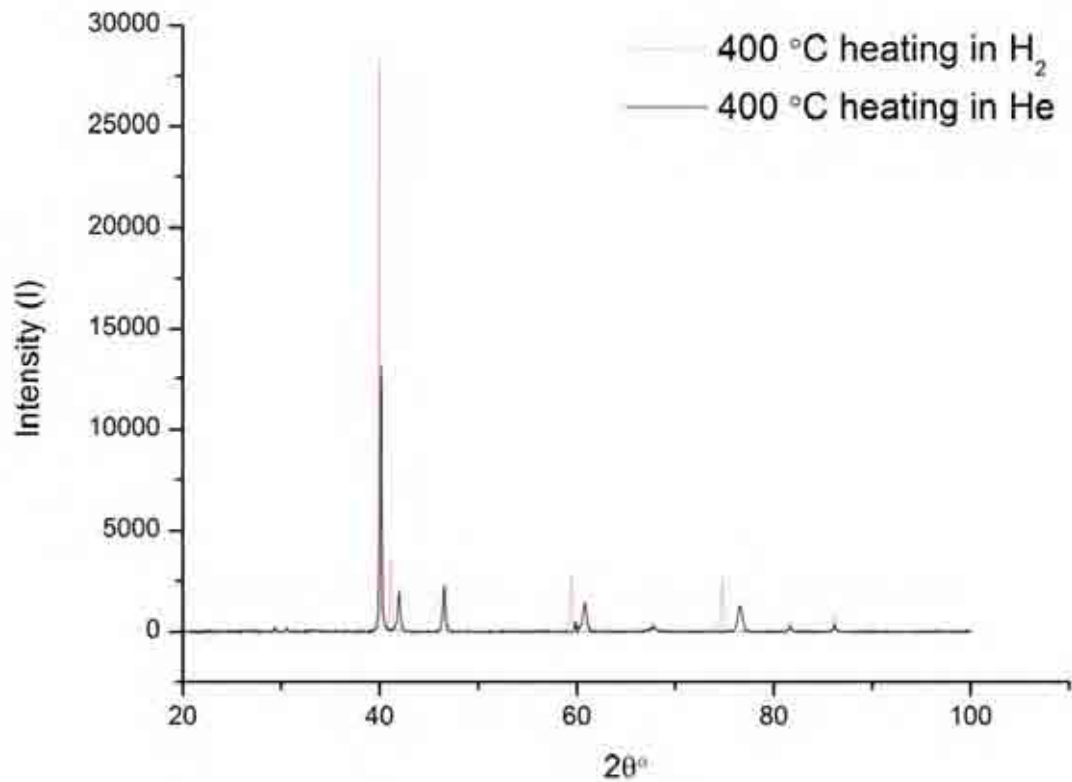


Figure 4.5: The effect hydrogen has in the membrane at 400 °C comparing to He for the same temperature.

Thus hydrogen will weaken the membrane as the solid solution of hydrogen inside vanadium will expand its lattice greatly and as it can be seen in Figure 4.4, the expansion will continue to increase even as we decrease temperature to the point where, at 320°C, the vanadium peak will overlap its neighbor peak meaning that the effect is time depended.

Also new peaks begin to form at 2θ 40.26 ° for 400 °C indicating the presence of Pd₃V which, as temperature rises, increases in intensity as more Pd₃V peak are formed at 33.16°, 47.09° for 550°C while at the same temperature the peak at 46.5° indicates the creation of Pd₂V which also increases in quantity at higher temperatures (Pd₂V peak at 68.63° for 600 °C). Again the creation of new alloys inside the membrane is not only temperature-related

but also time- dependent as, during cooling, more alloy peaks are formed. Thus for the pattern of the final temperature of 320 °C, the V peaks at 2θ 59.07° and 74.21° split into two and three peaks respectively. The first peak splits into a V peak at 59.019° and one Pd₂V at 60 .89° .The second peak splits into one V peak at 74.24°, one Pd₂V at 72.69° and one Pd₃V at 75.64°.

The disappearance of the last two and less intensive Pd peaks as the time pass can also be seen as an indication of the increase in Pd base alloys.

4.1.2 Hydrogen Permeability measurements

The measurements started after the system reached a temperature of 300°C (heated under He) where according to H-Pd and H-V phase diagrams no hydride phases exists. After that hydrogen enters the system with partial pressures of $P_1= 0.5$ and $P_2= 0$ bar or absolute pressures of $P_1 = 1.5 * 10^5$ Pa and $P_2 = 10^5$ Pa

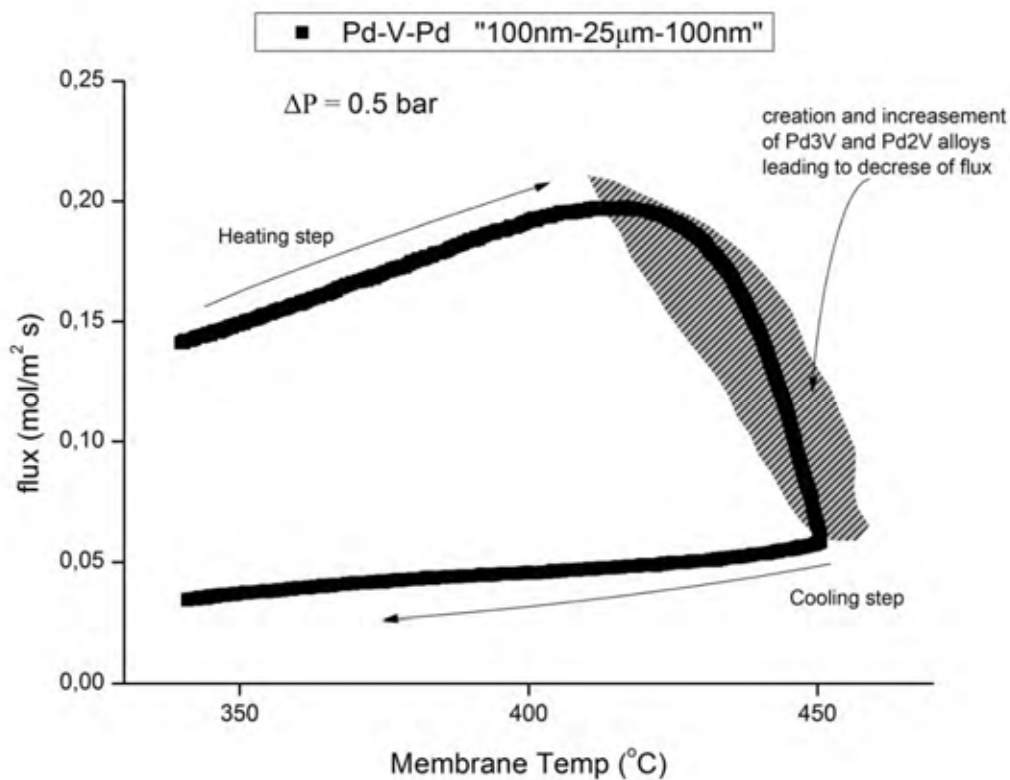


Figure 4.6: Hydrogen flux versus temperature for the 100 nm Pd coated 25 μm thick V membrane.

The membrane initially exhibited very high hydrogen flux, as shown in Figure 4.6; flux continues to increase until 410 °C before decreasing rapidly.

As shown in the XRD patterns of the membrane for temperatures above 400 °C in the presence of H_2 the creation of Pd_3V and Pd_2V is favoured, which also mean that the palladium on the membrane surface begins to diffuse into the vanadium. Thus two factors lead hydrogen flux to drop, first the catalytic ability that palladium gives to the membrane is decreased leading to the need of greater activation energies and second the creation of Pd-V alloys in the interface of the membrane that have low hydrogen permeability[39].

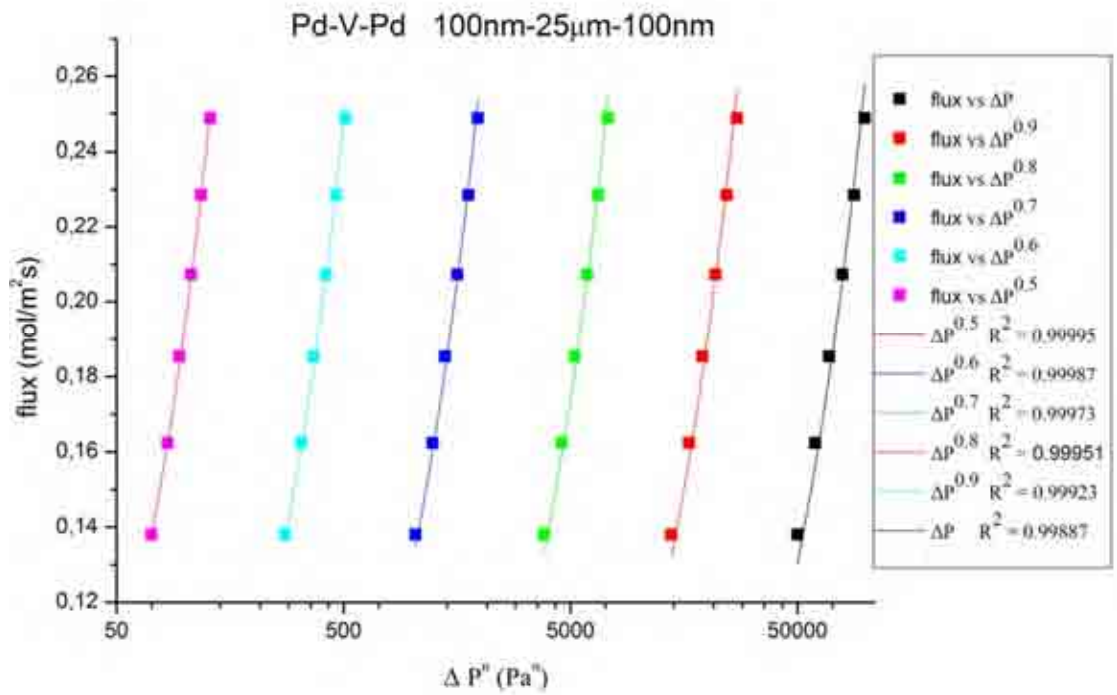


Figure 4.7: Hydrogen Flux vs ΔP^n at the beginning of hydrogen permeability measurement (330 °C heating)

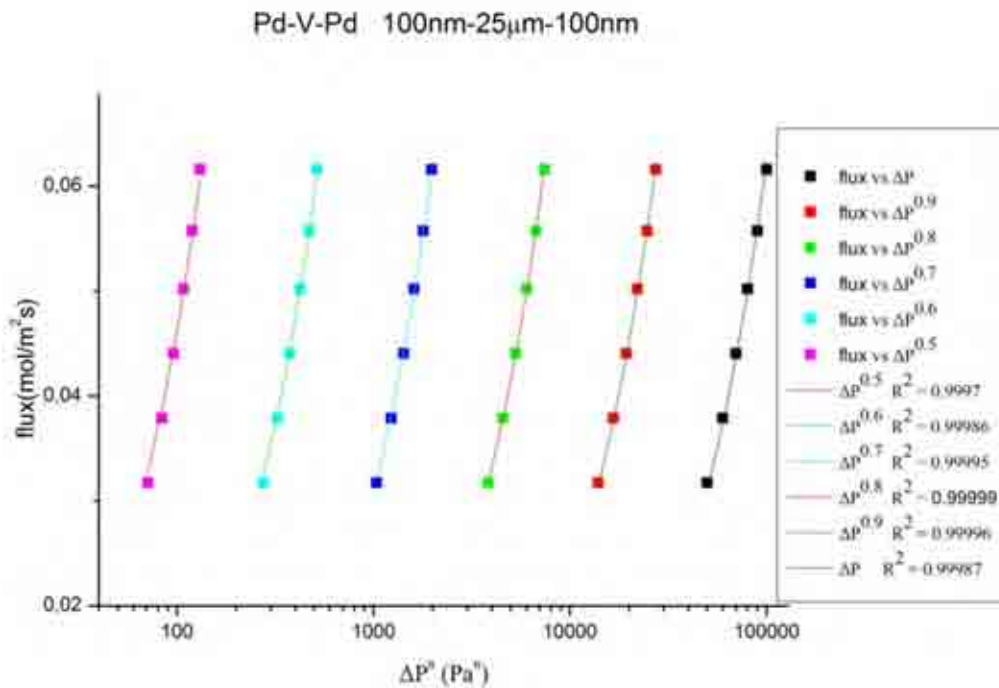


Figure 4.8: Hydrogen Flux vs ΔP^n at the end of hydrogen permeability measurement (330 °C cooling path from 450 °C)

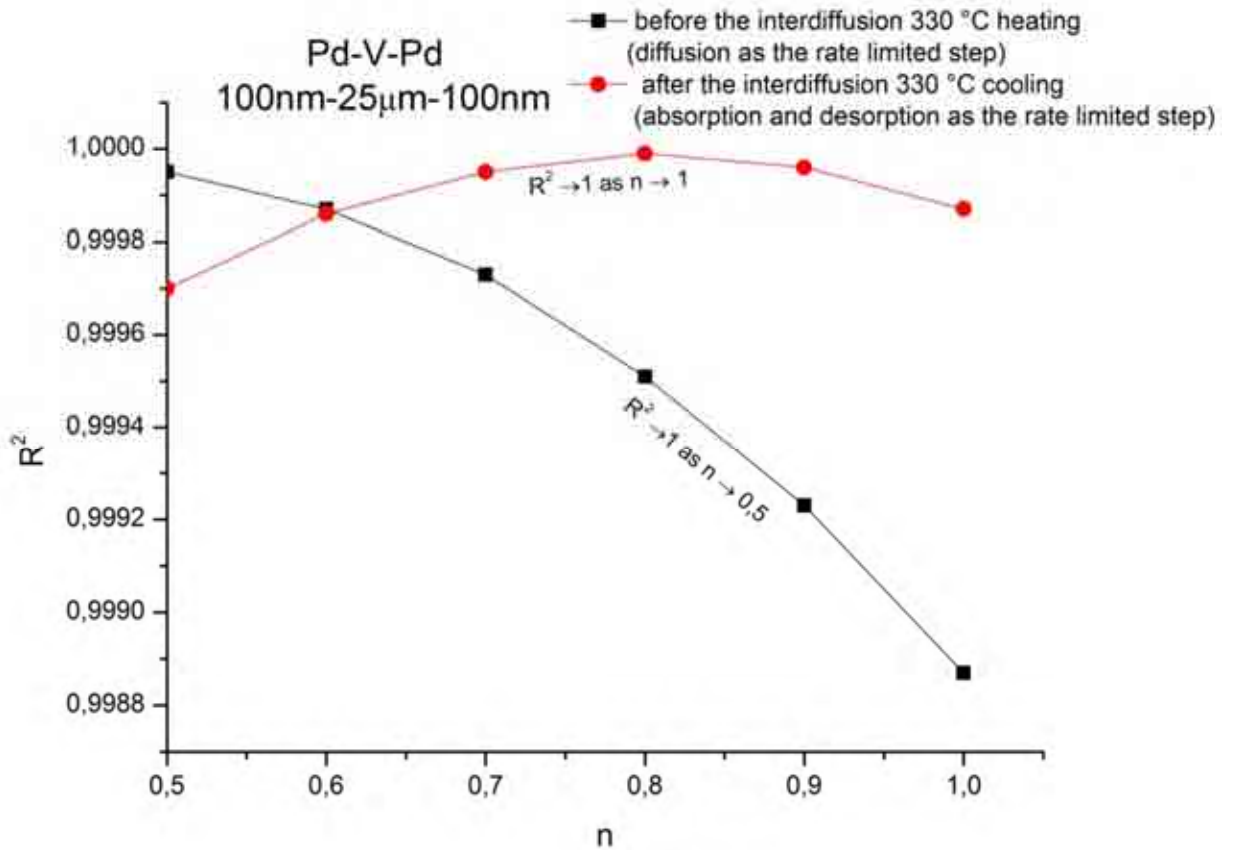


Figure 4.9: R^2 vs. n Pd-V-Pd with 100 nm of Pd at 330 °C during heating and cooling paths.

Figures 4.7-4.9 represents the isothermal measurements as mentioned in section 3.7.

At the beginning of the measurement, the membrane follows Sieverts' law as the equation that best fit the data for ΔP^n is that for $n=0.5$. On the other hand over 410 °C as palladium starts to diffuse into vanadium a deviation from Sieverts' law occurs, as can be seen in Figure 4.8 at 330 °C during cooling the best fit for n now is 0.8 so hydrogen flux changes from $J = \Phi \cdot (P_1^{0.5} - P_2^{0.5})/t$ that Sieverts' law suggest to $J = \Phi \cdot (P_1^{0.8} - P_2^{0.8})/t$ a result not valid according to Sieverts' law. Thus the single phenomenon of Pd diffusion into V leads to a number of other phenomena that ultimately result to the decrease of hydrogen flux.

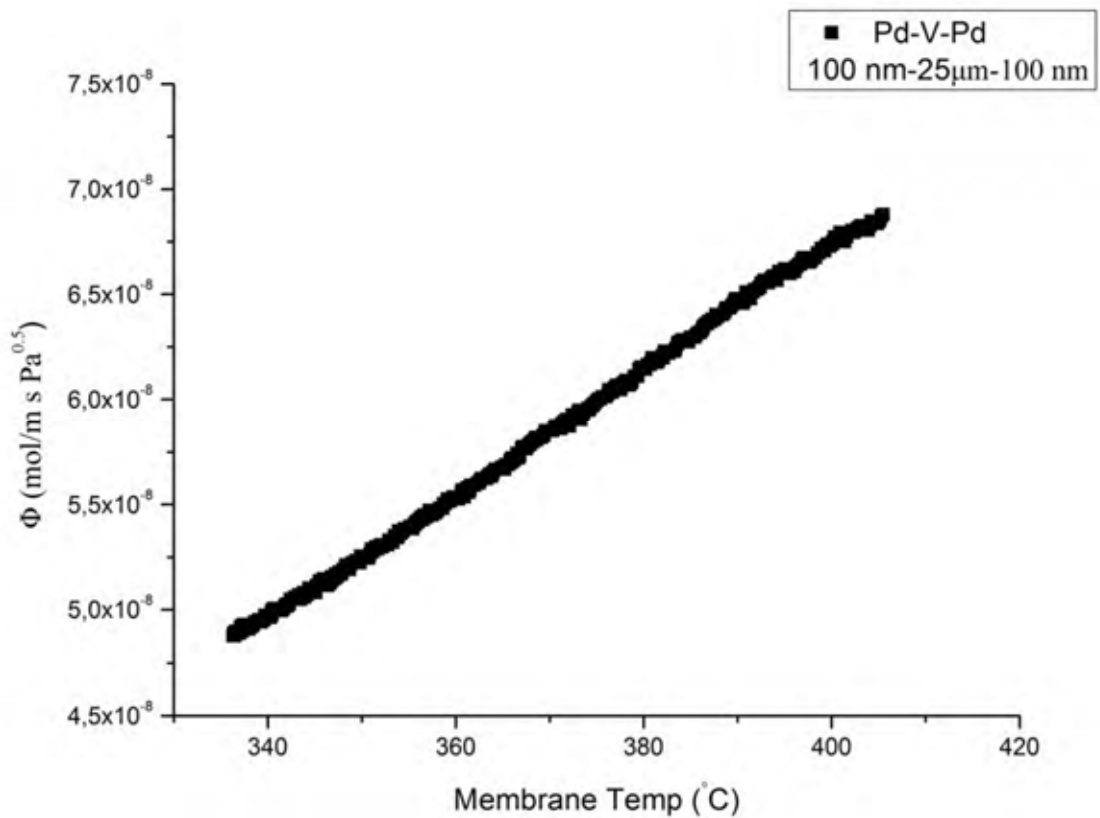


Figure 4.10: Hydrogen permeability (Φ) for the part where Sievert' law is applied (330°C - 410°C)

Using the data from the temperature range where Sieverts' law applies, hydrogen permeability is found to be much higher than for Pd-Ag membranes. Using these data the activation energy for hydrogen permeation can be found using Equation 2.5.

$$\Phi = K_s \exp(-E/RT) \Rightarrow \ln(\Phi) = \ln(K_s) - E/RT$$

By plotting these data using the above equation, the best possible linear function that can fit the data is $y = 17463.99x - 13.3897$ with $R^2 = 0.99932$, so the activation energy for this membrane is

17.46399 kJ/mol, while $\ln(K_S)$ is -13.3897 or $K_S = 1.53 \cdot 10^{-6} \text{ [mol} \cdot \text{Pa}^{0.5} \text{]}/\text{m}^2$

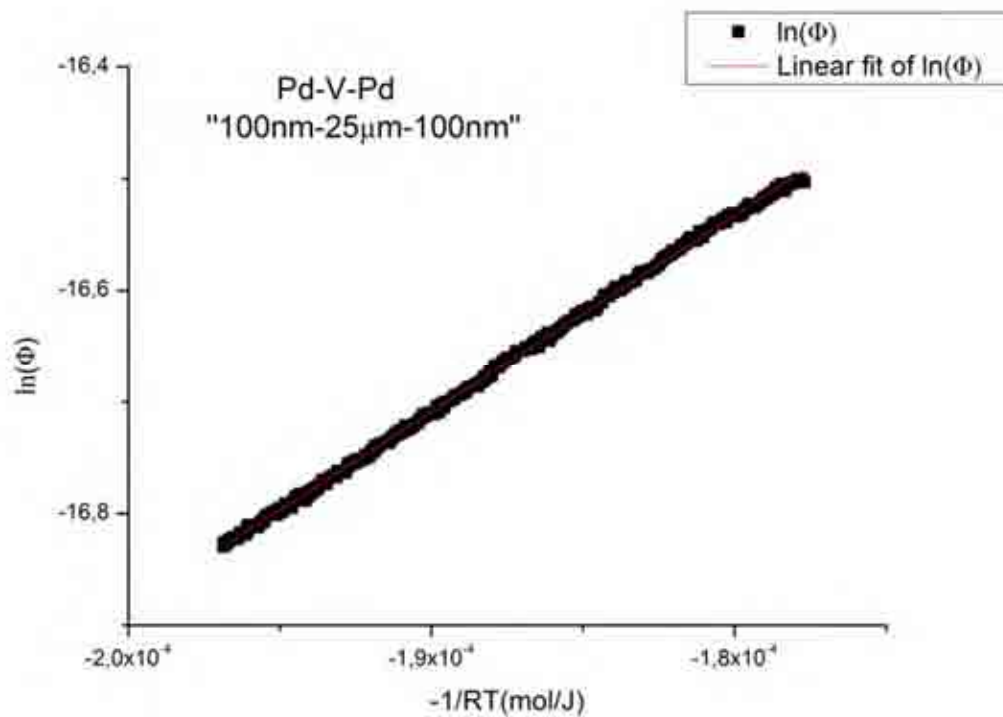


Figure 4.11: $\ln(\Phi)$ versus $-1/RT$ and the linear fit for the temperature range where Sieverts' law applies

The same measurements were executed for a 200 nm layer of Pd.

Again with the same conditions used for the membrane with the 100 nm Pd layer mentioned above we have the following flux diagram.

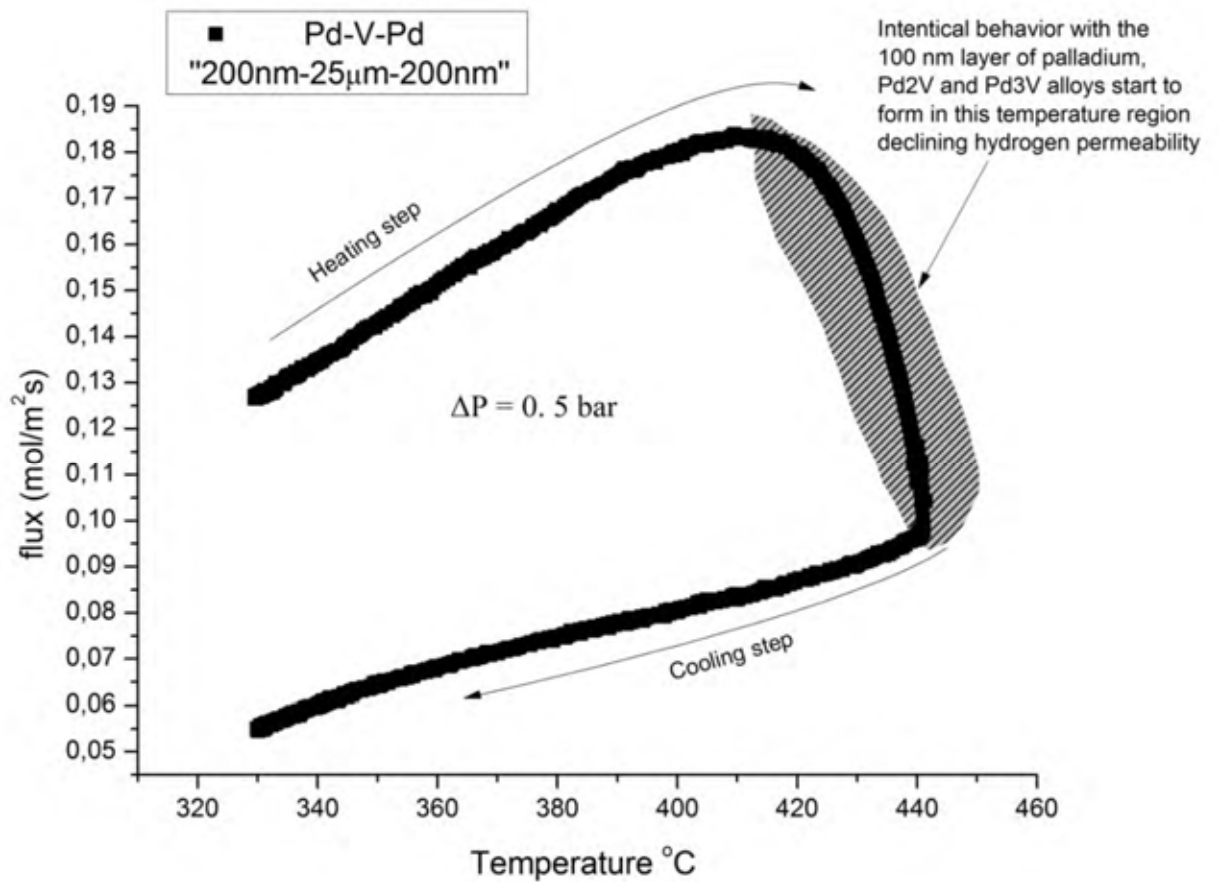


Figure 4.12: Hydrogen flux versus temperature for the 200 nm Pd coated 25 µm thick V membranes.

As can be seen in Figure 4.12, hydrogen flux remains at the same level measured for the 100 nm Pd. Also the behavior of the membrane seems to be the same without any significant variation. Again the flux increases until the system reaches a temperature of about 410°C from which point the flux begins to fall.

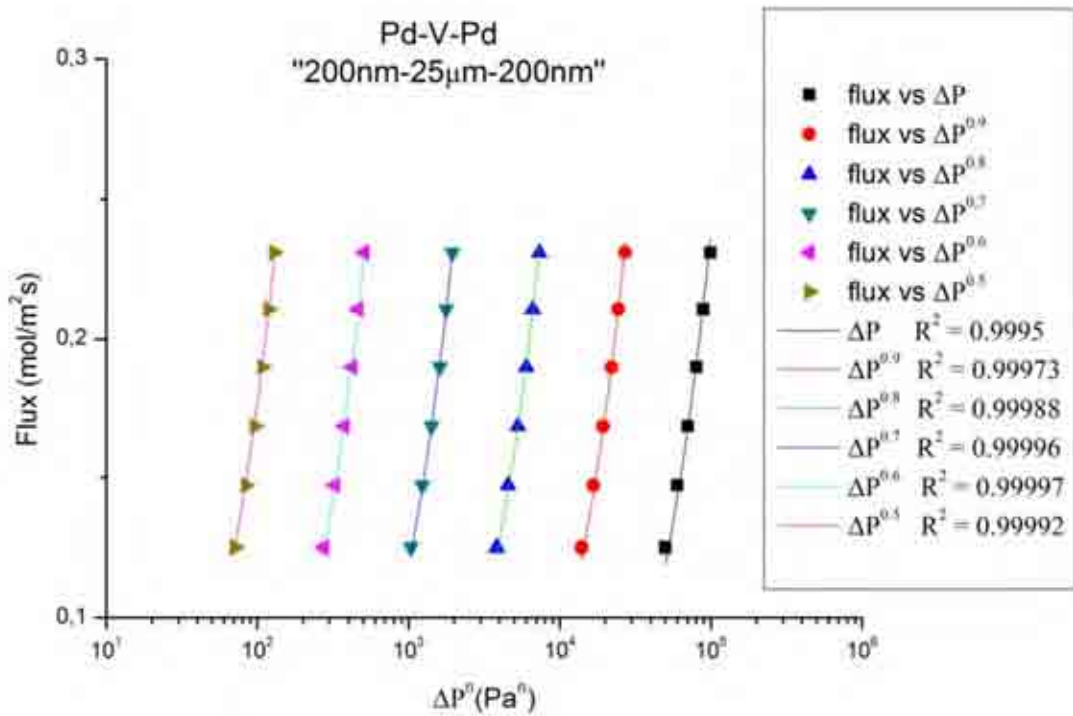


Figure 4.13: Hydrogen Flux vs ΔP^n at the beginning of hydrogen permeability measurement (330 °C heating)

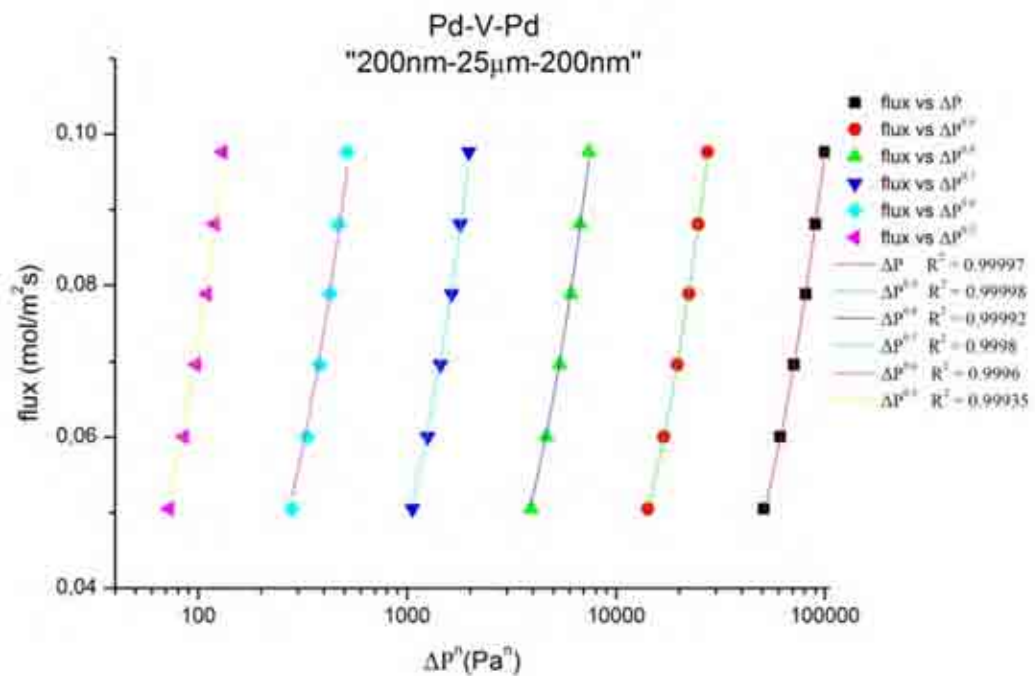


Figure 4.14: Hydrogen Flux vs ΔP^n at the end of hydrogen permeability measurement (330 °C cooling path from 450 °C)

This time at the beginning of hydrogen permeability measurement there is a small variation from Sieverts' law. As can be seen in Figure 4.13 now the best fit for n is 0.6 thus for the part where flux is increasing, the formula is $J = \Phi \cdot (P_1^{0.6} - P_2^{0.6}) / t$.

Again for temperatures above 410°C due to the intermetallic diffusion of Pd into V, flux decreases as the deviation from Sieverts' law increases during cooling path at 330°C.

During cooling the best fit for n is now 0.9 as it can be seen in Figure 4.14.

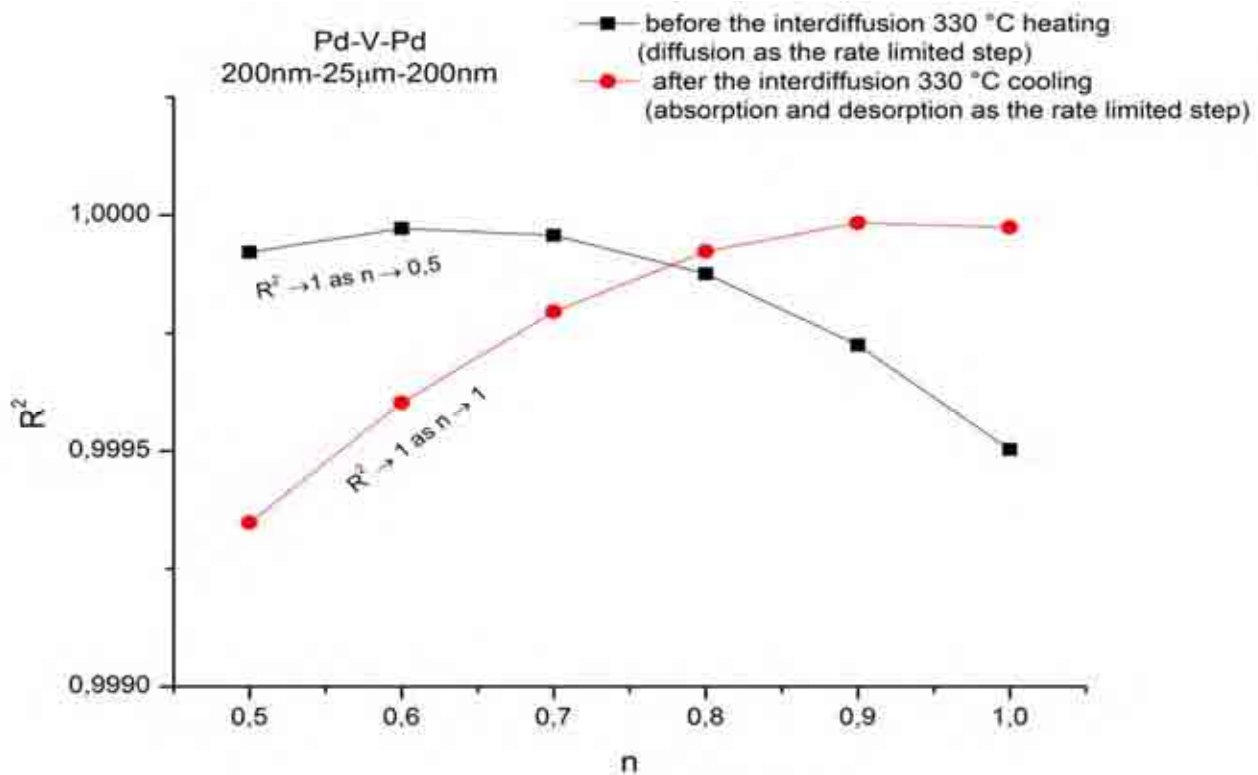


Figure 4.15: R^2 vs. n Pd-V-Pd with 200 nm of Pd at 330 °C during heating and cooling paths.

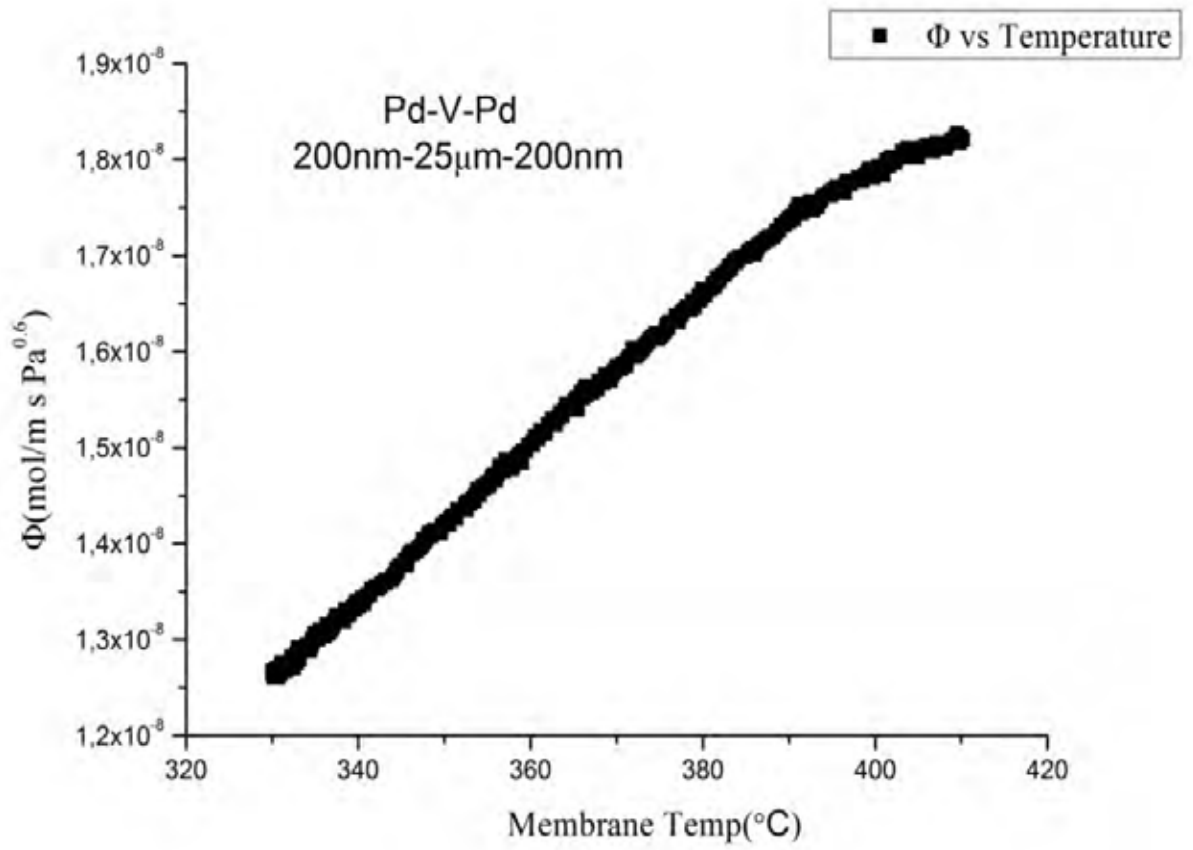


Figure 4.16: Hydrogen permeability (Φ) for the linear part where flux increases.

Using the flux data for the temperature range where flux increases linear we can see that hydrogen permeability for the 200 nm coating Pd-V-Pd is decreased in comparison to the 100 nm coating Pd-V-Pd but still remain in high levels. The decrease can be attributed to the fact that Sieverts' law deviates from $n=0.5$

Using permeability data for $n = 0.6$ this time, we take the diagram below.

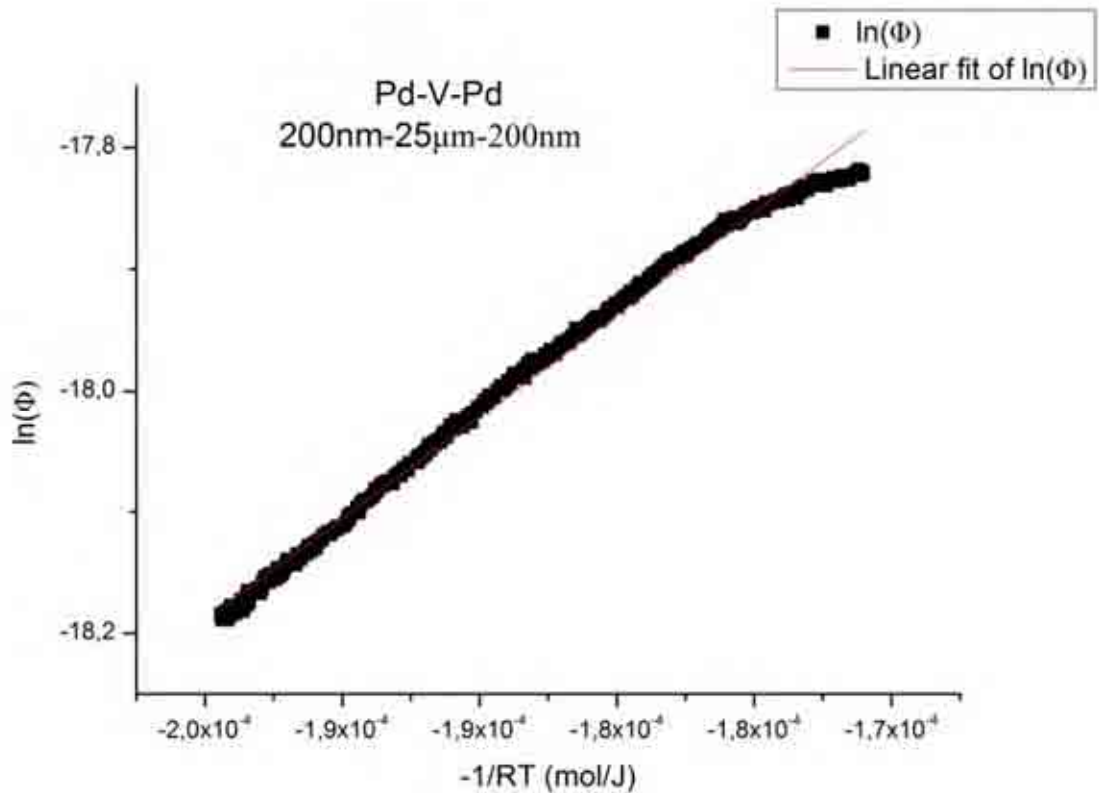


Figure 4.17: $\ln(\Phi)$ versus $-1/RT$ and the linear fit for the same temperature range that permeability was measured .

The linear function that best fits the above graph with $R^2 = 0.99316$ is:

$$y = -14.82906 + 16802.60x$$

Thus the activation energy of permeation for this membrane is $E = 16802.60$ J/mol or 16.80260 kJ/mol and $\ln(K_S) = -14.82906$ or $K_S = 3.6292 \cdot 10^{-7}$ [mol*Pa^{0.5}]/m². The activation energy has decreased by 3.94% in comparison to the previous membrane. Even Pd used in

this membrane is more we can't conclusively say that this extra Pd is responsible for the decrease in activation energy as more membranes with different Pd thicknesses need to be tested before a conclusion is made.

Also both of the Pd-V-Pd membranes above after tested for hydrogen permeability were shown to be very fragile.

4.2 Pd-Nb-Pd

As Niobium and Pd will form hydride phases at temperatures below 300 °C the system was first heated under helium before the introduction of hydrogen inside hydrogen permeability apparatus.

Hydrogen permeability measurements for the Pd-Nb-Pd membranes were problematic due to high rates of membrane failure when exposed to hydrogen. Hydrogen was admitted above 300°C using a pressure ramp rate of 0.005 bar a sec until a final pressure of 1 bar was reached.

To investigate this phenomenon, Pd-Nb-Pd was also characterized with the use of in situ XRD in the presence of both He and H at the same temperatures and pressures in order to replicate the conditions at which the membranes failed.

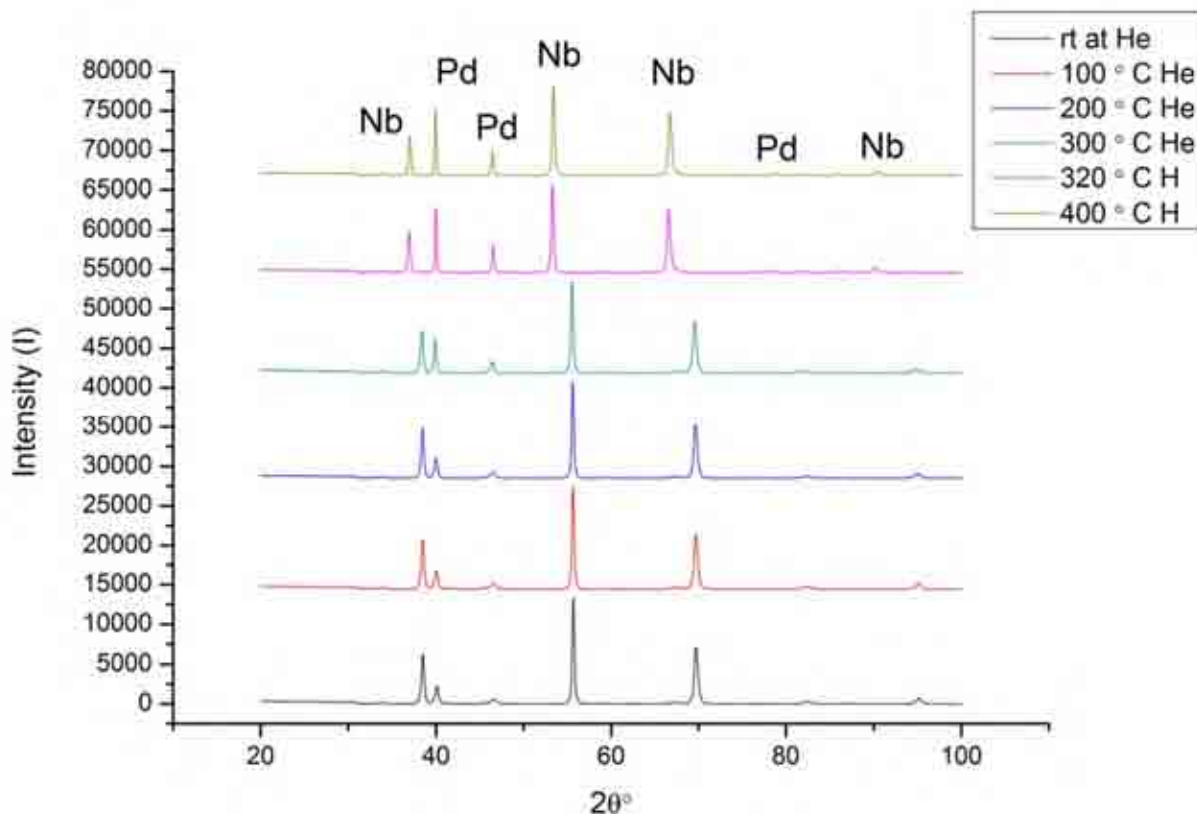


Figure 4.18: XRD pattern of Pd-Nb –Pd for various temperatures in the presence of He and H₂.

X-ray diffraction patterns in Figure 4.18 show that niobium peaks remains fairly steady while the membrane is being heated under He but in the presence of H a significant shift occurs in all Niobium peaks suggesting that the collapse of Pd-Nb-Pd membranes is a result of the Niobium lattice being expanded. Hydrogen solubility inside niobium is too great and as the membrane operates with pressure a solubility gradient across the membrane is present and therefore an expansion gradient. On the other hand Pd remains stable in the presence of both He and H as the shift of Pd peaks are trivial while an increasement of intensities as the temperatures go up is observed.

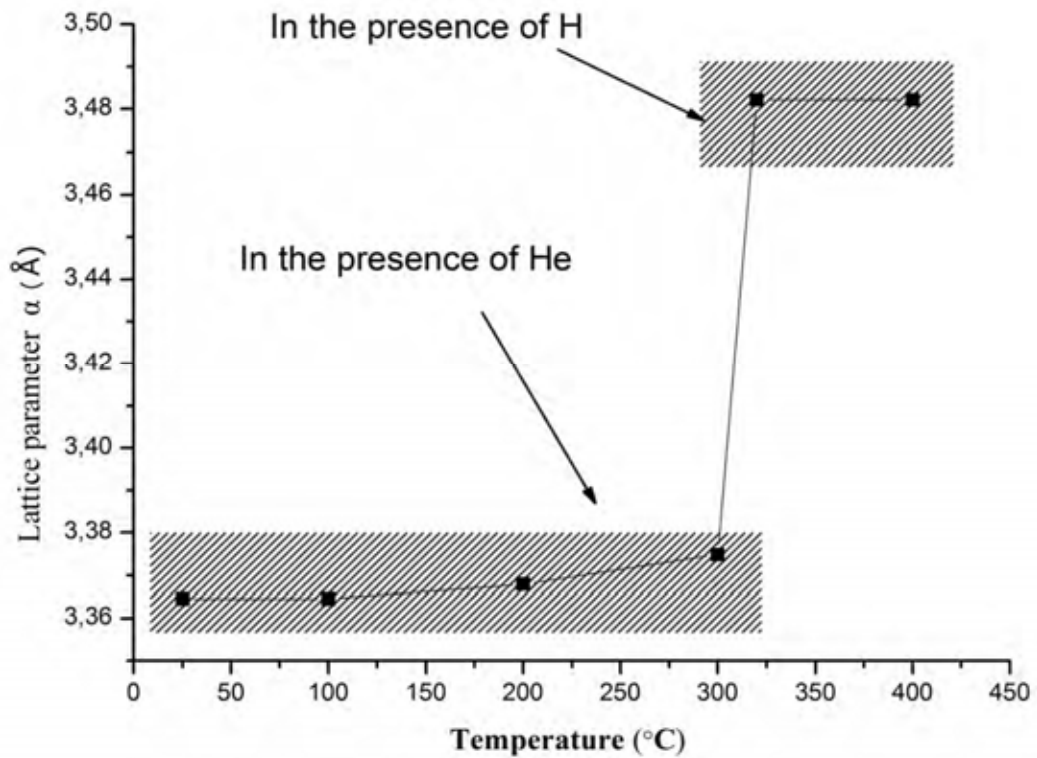


Figure 4.19: The increase of Nb lattice parameter as the temperature increases and H enters the lattice. (Lattice parameters of the diagram are the mean of lattice parameters calculated for each peaks and temperature)

Calculating the lattice parameters at each temperature reveals how large is the hydrogen solubility for niobium, resulting in the expansion of niobium lattice, as for just 20°C α increases by 3.17%. On the other hand while the membrane is heated under He between room temperature and 300°C, lattice parameter α change by only 0.31%. This non-uniform in nature expansion of niobium that causes cracks and defects is the reason resulting in failure

4.3 Permeability comparison between Pd , PdAg, and Pd-V-Pd membranes

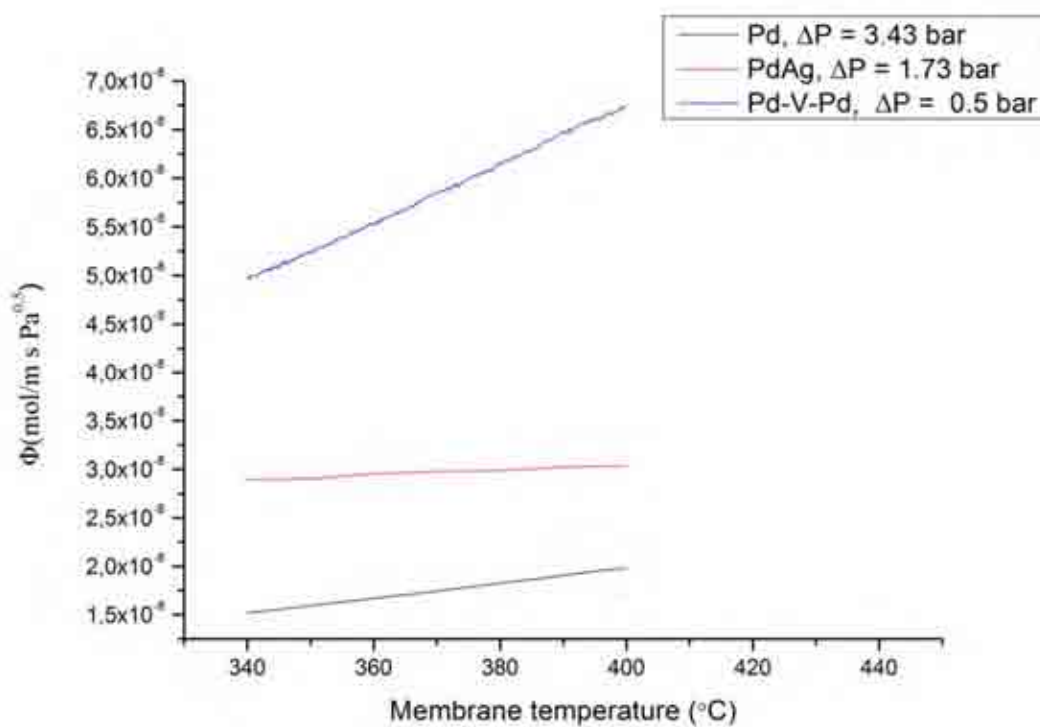


Figure 4.20: Hydrogen permeability comparison between a Pd a PdAg and a Pd-V-Pd membrane.

As we can see at the figure 4.20 above is obvious that the V based membrane can achieve much greater hydrogen permeability in comparison to the current commercial standard PdAg membranes

The data for the V based membrane are those from the Pd-V-Pd membrane with the 100 nm palladium layer as for that membrane Sieverts' law was better applied.

4.4 Stability measurement

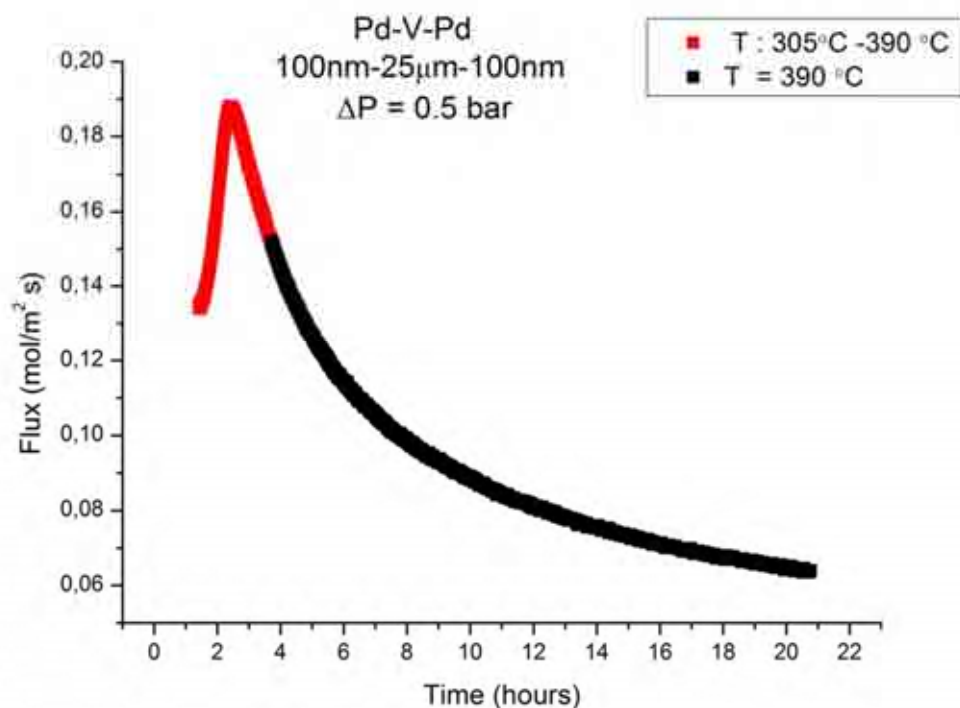


Figure 4.21: Flux against time at 390 °C and 0.5 bar ΔP

As with previous permeability measurements, the membrane is first heated until it reaches 300 °C before H₂ enter the system. As can be seen in Figure 4.21 by the time the system reached 390°C at which it was going to left, maximum flux is already reached and decrease of flux has begun.

Taking into account the results from XRD patterns, the membrane behavior can be attributed to the diffusion of Pd inside V and thus the creation of Pd-V alloys that decrease hydrogen flux. The

fact that flux isn't stabilized but keeps decreasing can verify that the phenomenon of interdiffusion is time dependent.

4.5 SS couples (SS-Pd and SS-V-Pd)

Due to the fact that during the time of SS couples measurements, the diffractometer introduced a contamination in the form of dynamic peaks (unstable as temperature change) the most intense peak of Pd at 39.90° is used as it contains the necessary information.

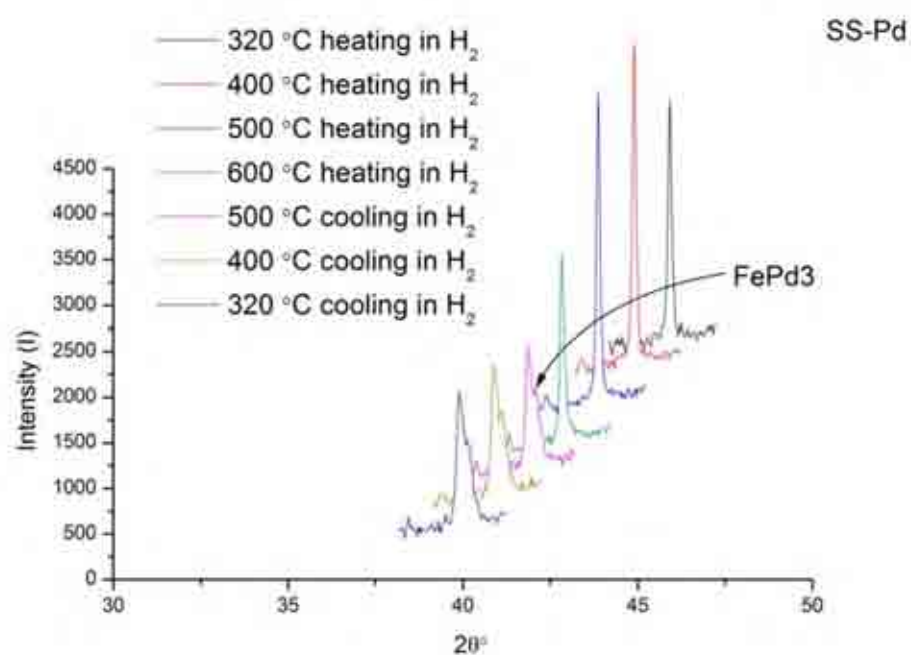


Figure 4.22: The most intense Pd peak of SS-V couple at different temperatures in the presence of 1 bar H₂

The SS couple coated with 200 nm of Pd remains stable until the highest temperature while during cooling the FePd₃ peak is formed as can be seen in Figure 4.22, but when a 100 nm layer of vanadium is coated between SS and Pd for the same peak and for the same conditions we have the following pattern.

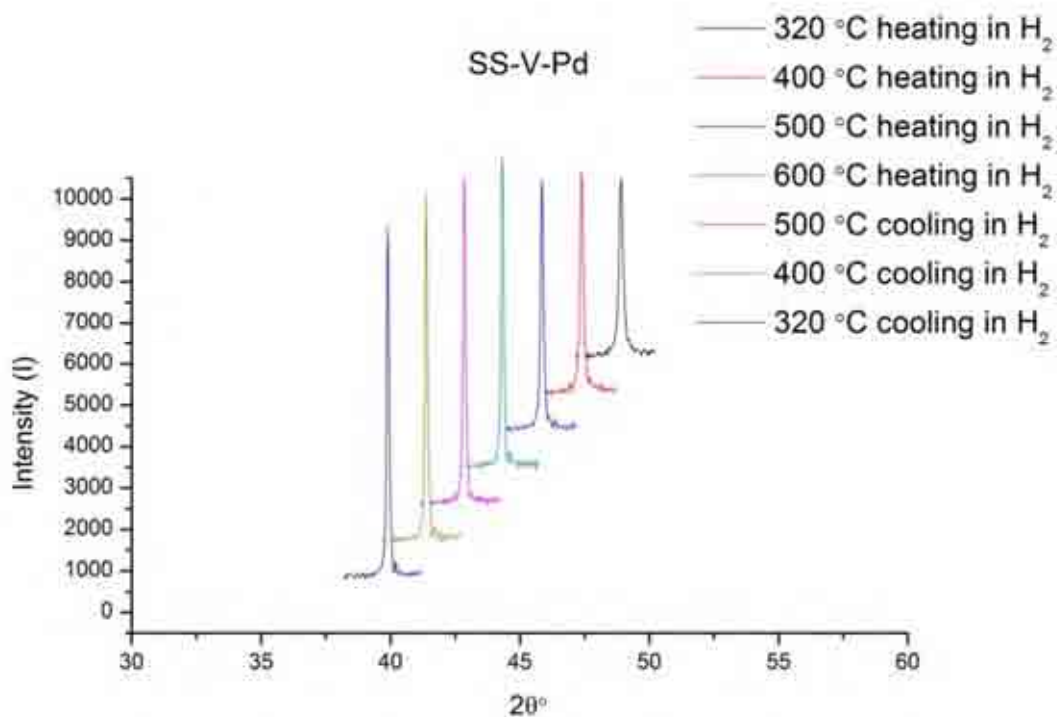


Figure 4.23: The most intense Pd peak of a SS-V-Pd system at different temperatures in the presence of 1 bar H₂

This, time the peak remains stable during the whole range of temperatures as the presence of vanadium blocks palladium to diffuse inside SS.

4.6 SEM investigation

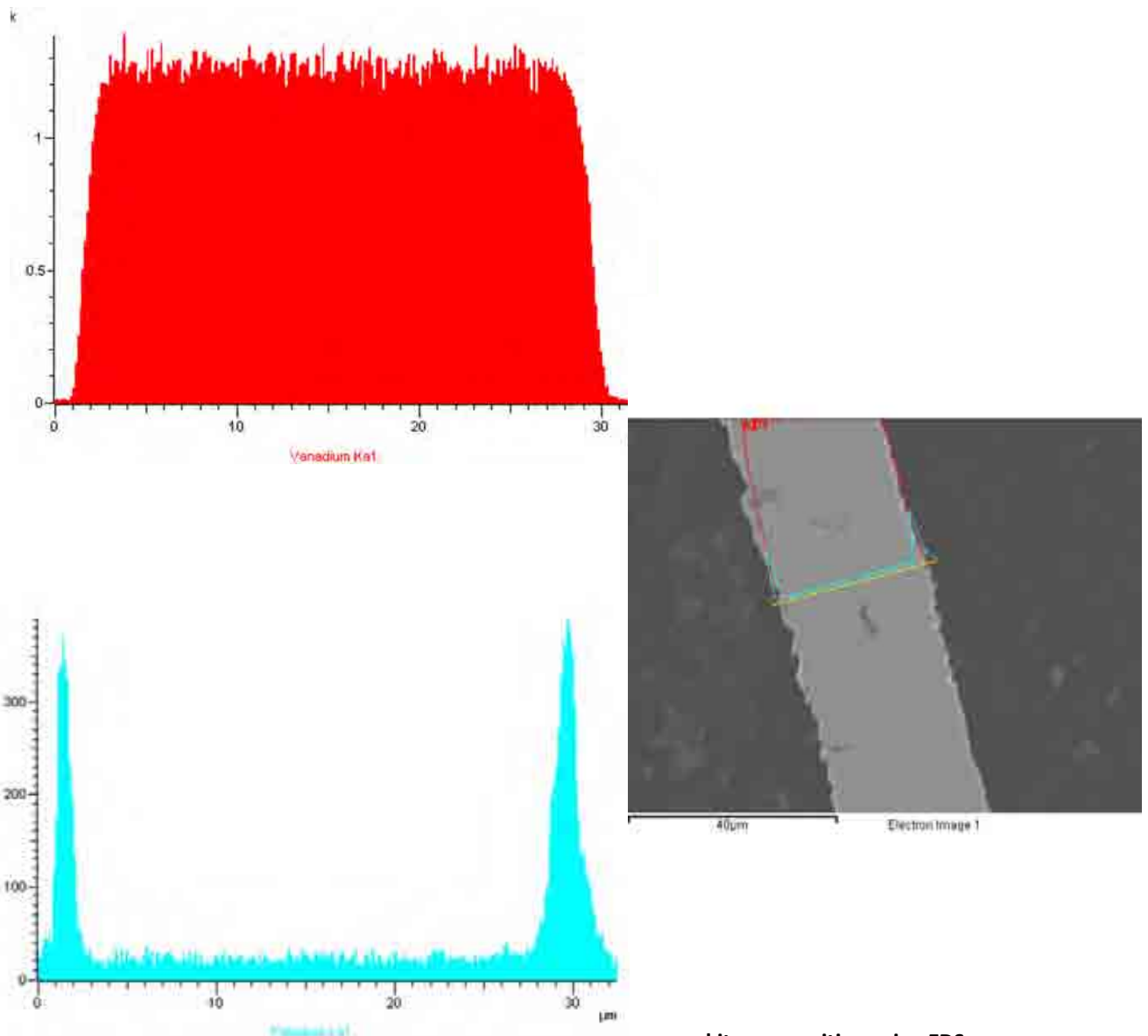


Figure 4.24: Cross-section of the Pd-V-Pd membrane and its composition using EDS

Using SEM EDS as it can be seen in Figure 4.24 the composition of the fabricated membrane was verified.

In the same manner a Pd-V-Pd membrane composition was explored after it has been tested in the hydrogen permeability apparatus. The membrane explored was the 100 nm Pd-V-Pd mentioned before. As can be seen at Table 4.1 EDS verifies the interdiffusion phenomenon of Pd inside vanadium that XRD show. Using the scale of the SEM picture in Figure 4.25 we can measure that Pd diffused up to 3 μm inside vanadium.

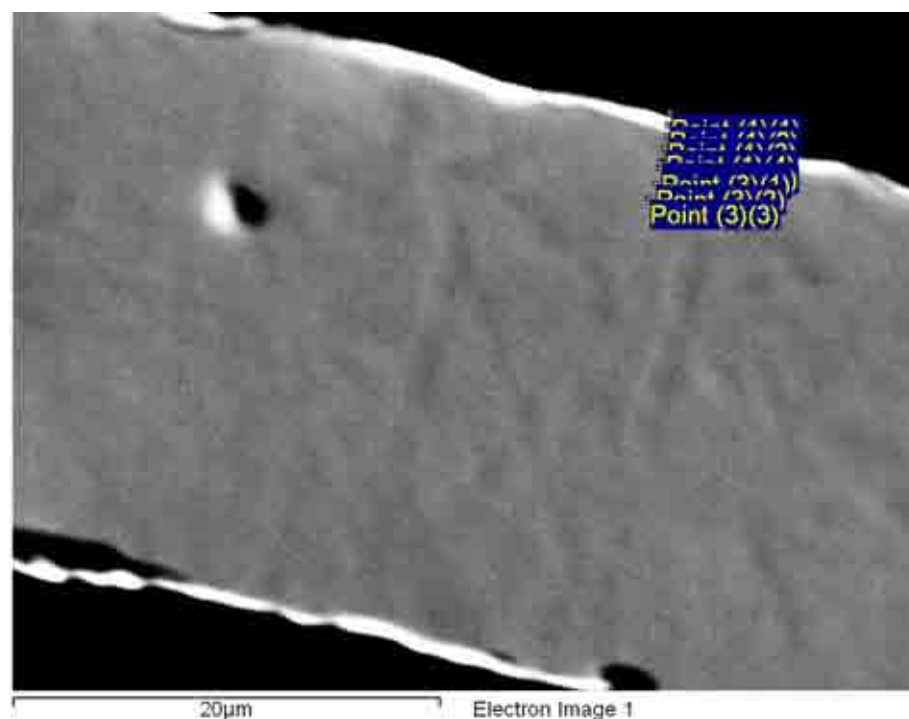


Figure 4.25: SEM cross-section of the 100 nm Pd-V-Pd membrane after the hydrogen permeability measurement. Few points from the surface to the inside of the membrane have been selected for EDS to scan.

| Spectrum | In stats. | V | Pd | Total |
|---------------|-----------|--------|-------|--------|
| Point (1)(1) | Yes | 26.86 | 73.14 | 100.00 |
| Point (1)(2) | Yes | 62.90 | 37.10 | 100.00 |
| Point (1)(3) | Yes | 89.46 | 10.54 | 100.00 |
| Point (1)(4) | Yes | 98.12 | 1.88 | 100.00 |
| Point (1)(5) | Yes | 99.47 | 0.53 | 100.00 |
| Point (2) (1) | Yes | 100.00 | | 100.00 |
| Point (3)(1) | Yes | 99.59 | 0.41 | 100.00 |
| Point (3)(2) | Yes | 100.00 | | 100.00 |
| Point (3)(3) | Yes | 100.00 | | 100.00 |
| Max. | | 100.00 | 73.14 | |
| Min. | | 26.86 | 0.41 | |

Table 4.1: Composition of each point shown in figure 4.22(All results in weight %)

4.7 General discussion

The coating of vanadium films with palladium removed the surface problem of vanadium, the data suggested that for both of the Pd-V-Pd membranes the rate limited step of hydrogen permeation was diffusion, thus hydrogen was able to permeate through vanadium following Sievert' law.

Both Pd-V-Pd membranes with the 100 nm and 200 nm thickness coating of Pd achieved high hydrogen permeabilities in the range that the literature would suggest, but that high hydrogen permeability isn't followed by duration of efficiency and stability of the membrane. For temperatures above 400°C, palladium starts to diffuse into vanadium creating V-Pd alloys that don't favor the permeation of hydrogen, making absorption and desorption the rate limited step of hydrogen permeation. Thus n is increased towards 1. Also the high solubility of hydrogen that vanadium has, causes the membrane to be weakened as a result of the expansion gradient that is formed inside the lattice of the membrane. That mean that V/H is very brittle.

Because niobium is expected to have higher hydrogen permeabilities than vanadium, hydrogen solubility is also higher. Thus a higher expansion gradient is formed during the operation of the membrane which caused the Pd-Nb-Pd membrane to collapse.

Also due to hydride phases that are formed for temperatures below 300°C for both vanadium and niobium, hydrogen must be used above that temperature. Thus the membrane has a very narrow range of operational temperatures between only 300°C and 400°C.

The vanadium barrier that is used in the SS-Pd couple was show to work very well as it manage to block palladium from being diffused into SS at high temperatures.

Chapter 5

Conclusions and further work

5.1 Conclusions

- Niobium thickness of 25 μm isn't enough to keep up with the expansion hydrogen causes to its lattice when pass through it over 300 $^{\circ}\text{C}$
- Coating a very thin layer of Pd over V activates vanadium surface for the permeation of H_2 through it.
- Vanadium can perform much better in comparison to Pd-Ag alloys based membranes.
- Pd will diffuse for temperatures close to 400 $^{\circ}\text{C}$ as a result the surface is deactivated and Pd-V alloys such as Pd₃V and Pd₂V are created causing a rapid decrease in hydrogen flux.
- Once Pd diffusion starts, it will keep diffusing even at temperatures below the threshold of diffusion much.
- The two thicknesses (100 and 200 nm) of Pd used don't seem to affect the performance of the membrane.

- Hydrogen causes Pd-V-Pd membranes mechanical instability as the solid solution that creates with vanadium expands its lattice and further use of the membrane after being used for one cycle isn't possible, vanadium films with thickness over 25 μm may solve this problem.
- A further investigation is needed but it seems that V can work very well as an interdiffusion barrier in a supported membrane.

5.2 Future work

1. Test more Pd thickness on vanadium and see if they really and in what way affect hydrogen permeability.
2. Calculate with more precision n value.
3. Further investigation of palladium interdiffusion inside vanadium and the alloys that are formed.
4. Increase the thickness of Niobium films and test them for their hydrogen permeability properties.
5. Increase the thickness of vanadium films in order to fabricate membranes that are more stable and can be used for more than one cycle in a hydrogen permeability measurement.
6. Study more complex vanadium ,Niobium based alloy systems (binary/ternary alloys like V-10Pd, V-9Ni, V-15Cu, Nb-1Zr, V-6Ni-5Co, V-9Ni-Co)
7. Further investigate the ability that vanadium seems to have as an inter-metallic barrier for diffusion.

Bibliography

1. Moss, T.S., et al., *Multilayer metal membranes for hydrogen separation*. International Journal of Hydrogen Energy, 1998. **23**(2): p. 99-106.
2. Phair, J.W. and R. Donelson, *Developments and design of novel (non-palladium-based) metal membranes for hydrogen separation*. Industrial & Engineering Chemistry Research, 2006. **45**(16): p. 5657-5674.
3. Buxbaum, R.E. and T.L. Marker, *Hydrogen transport through non-porous membranes of palladium-coated niobium, tantalum and vanadium*. Journal of Membrane Science, 1993. **85**(1): p. 29-38.
4. Eric M. Goodger, L.P., *Transport Fuels Technology: mobility for the millenium*. 2000.
5. Nathan W. Ockwig, T.M.N., *Membranes for Hydrogen Separation* Chemical Reviews 2007. **107**: p. 4078-4110.
6. Muradov, N.Z. and T.N. Veziroglu, *"Green" path from fossil-based to hydrogen economy: An overview of carbon-neutral technologies*. International Journal of Hydrogen Energy, 2008. **33**(23): p. 6804-6839.
7. Wiessner, F.G., *Basics and industrial applications of pressure swing adsorption (PSA) , the modern way to seperrate gas* Gas Separation and Purification 1988. **2**: p. 115-119.

8. Paglieri, S.N. and J.D. Way, *INNOVATIONS IN PALLADIUM MEMBRANE RESEARCH*. Separation & Purification Reviews, 2002. **31**(1): p. 1 - 169.
9. University of California - Los Angeles (2009, O., Scientists Report. ScienceDaily. . *Last Time Carbon Dioxide Levels Were This High: 15 Million Years Ago*. 2009; Available from: <http://www.sciencedaily.com/releases/2009/10/091008152242.htm>.
10. *KYOTO PROTOCOL TO THE UNITED NATIONS FRAMEWORK CONVENTION ON CLIMATE CHANGE*. 1998, UNITED. NATIONS.
11. Holladay, J.D., et al., *An overview of hydrogen production technologies*. Catalysis Today, 2009. **139**(4): p. 244-260.
12. Mathias, P. 2003: Tokyo p. 68th Annual Meeting of the Society of Chemical Engineers.
13. Brian M. Besancon , V.H., Raphaelle Imbault-Lastapis, Robert Benesch, Maria Barrio, Mona J. Molnvik, *Hydrogen quality from decarbonized fossil fuels to fuel cells* International Journal of Hydrogen Energy, 2009. **34**: p. 2350-2360.
14. Cicconardi, S.P., A. Perna, and G. Spazzafumo, *Combined power and hydrogen production from coal. Part B: Comparison between the IGHP and CPH systems*. International Journal of Hydrogen Energy, 2008. **33**(16): p. 4397-4404.
15. Commission of the European, C., *Non-fossil derived hydrogen in coal conversion processes : a further study*. 1982: CEC.
16. Perna, A., *Combined power and hydrogen production from coal. Part A--Analysis of IGHP plants*. International Journal of Hydrogen Energy, 2008. **33**(12): p. 2957-2964.
17. Kalinci, Y., A. Hepbasli, and I. Dincer, *Biomass-based hydrogen production: A review and analysis*. International Journal of Hydrogen Energy, 2009. **34**(21): p. 8799-8817.
18. DOE. Available from: http://www1.eere.energy.gov/hydrogenandfuelcells/fuelcells/fc_types.html.

19. Dicks, A.L., *Hydrogen generation from natural gas for the fuel cell systems of tomorrow*. Journal of Power Sources. **61**(1-2): p. 113-124.
20. Huang, C., et al., *On-board removal of CO and other impurities in hydrogen for PEM fuel cell applications*. Journal of Power Sources, 2006. **162**(1): p. 563-571.
21. Adhikari, S. and S. Fernando, *Hydrogen membrane separation techniques*. Industrial & Engineering Chemistry Research, 2006. **45**(3): p. 875-881.
22. Pyle, W. *Hydrogen Purification*. Home power 1998 67]; 42-49].
23. Ma, Y.H. and F. Guazzone, *Metallic membranes for the separation of hydrogen at high temperatures*. Annales De Chimie-Science Des Materiaux, 2007. **32**(2): p. 179-195.
24. Sholl, D.S. and Y.H. Ma, *Dense Metal Membranes for the Production of High-Purity Hydrogen*. MRS Bulletin, 2006. **31**(10): p. 770-773.
25. Wang, Z.M., V. Li, and S.L.I. Chan, *Review of alloy membranes/film for hydrogen separation or purification*. Journal of Rare Earths, 2005. **23**: p. 611-616.
26. William J. Koros, R.M., *Pushing the limits on possibilities for large scale separation: which strategies* Journal of Membrane Science, 2000. **175**: p. 181-196.
27. al., Y.S.e., *Development of membrane reformer system for highly efficient hydrogen production from natural gas*. International Journal of Hydrogen Energy, 2009.
28. Nathan W. Ockwig, T.M.N., *Membranes for Hydrogen Separation* Chemical Reviews, 2007. **107**: p. 4078-4110.
29. Alefeld, G. and J. Völkl, *Hydrogen in metals I : basic properties*. Topics in applied physics. 1978, Berlin (etc): Springer.
30. Christmann, K., *Some general aspects of hydrogen chemisorption on metal surfaces*. Progress in Surface Science. **48**(1-4): p. 15-26.
31. Nørskov, J.K. and F. Besenbacher, *Theory of hydrogen interaction with metals*. Journal of the Less Common Metals, 1987. **130**: p. 475-490.

32. Wipf, E.b.H., et al., *Hydrogen in Metals III Properties and Applications*. 1997: Springer-Verlag Berlin Heidelberg 1997.
33. S.A.Steward, *Review of HydrogenIsotope Permeability Through Materials*. 1983.
34. Kolachev, B.A., *Hydrogen embrittlement of nonferrous metals*. 1968, Jerusalem: Israel Program for Scientific Translations.
35. Alefeld, G. and J. Völkl, *Hydrogen in metals II : application-oriented properties*. Topics in applied physics. 1978, Berlin: Springer. xxii,387p.
36. *UDP 350-4 DIFFUSION PUMP DC POWER SUPPLY PLATING SYSTEM INSTRUCTION MANUAL, TEER COATINGS LTD,2007*
37. *Confocal Scanning Laser Microscope LEXT OLS3000 User's manua ,OLYMPUS*
38. Chater, F., *Introduction to X-RAY Diffraction and the D8*.
39. David J. Edlund , J.M., *The relationship between intermetallic diffusion and flux decline in composite-metal membranes implications for achieving long membrane lifetime Journal of Membrane Science 1995. 107: p.147-153*